DOE/MC/30012 -- 5134
(DE96004357)

Advanced Sulfur Control Concepts In Hot-Gas Desulfurization Technology

Quarterly Report
July - September 1995

Douglas P. Harrison

October 1995

Work Performed Under Contract No.: DE-AC21-94MC30012

For
U.S. Department of Energy
Office of Fossil Energy
Morgantown Energy Technology Center
Morgantown, West Virginia

By
Louisiana State University
Baton Rouge, Louisiana

DISCLAIMER

DOE/MC/30012 -- 5134
(DE96004357)
Distribution Category UC-106

Advanced Sulfur Control Concepts In Hot-Gas Desulfurization Technology

Quarterly Report
July - September 1995

Douglas P. Harrison

Work Performed Under Contract No.: DE-AC21-94MC30012

For
U.S. Department of Energy
Office of Fossil Energy
Morgantown Energy Technology Center
P.O. Box 880
Morgantown, West Virginia 26507-0880

By
Louisiana State University
Department of Chemical Engineering
Baton Rouge, Louisiana 70803

October 1995

EXECUTIVE SUMMARY

Both the Antek total sulfur analyzer and the modifications to the Shimadzu GC-14A gas chromatograph to be used for analysis for SO_2 and H_2S were delivered during the quarter. Problems were faced during the installation and calibration phases of both instruments. By the end of the quarter we believe that the GC problems have been solved, but problems remain with the Antek analyzer. It appears that too much sulfur (as SO_2) reaches the UV detector and causes it to become saturated. This shows up as a maximum in the instrument calibration curve. At 200 psia, the capillary flow restrictor allows a total flow rate of about 180 sccm, and the maximum occurs at about 1% H_2S in the calibration gas. Reducing the pressure so that the total flow is reduced to about 25 sccm shifts the calibration curve maximum to about 5.7% H_2S. It appears that we must reduce the total flow rate to the detector or provide additional dilution. This may be accomplished by increasing the resistance of the capillarly restrictor, by diverting a portion of the flow leaving the pyrotube to vent, or adding an inert such as N_2 to the gases exiting the pyrotube. We are in contact with Antek representatives about the problem.

Both the atmospheric pressure and high pressure electrobalances were used during the quarter to study the regeneration of FeS in atmospheres of O_2/N_2 or H_2O/N_2. In the atmospheric pressure unit the effects of temperature (600 - 800°C), flow rate (130 - 500 sccm), and reactive gas mol fraction (0.005 to 0.03 O_2 and 0.1 to 0.5 H_2O) are being studied. Regeneration tests completed to date in the high pressure unit have utilized only O_2/N_2 and the parameters studied include temperature (600 - 800°C), flow rate (500 - 1000 sccm), pressure (1 - 15 atm) ad O_2 mol fraction (0.005 - 0.03).

In an oxygen atmospheres, the desired reaction is

$$2FeS(s) + \frac{7}{2}O_2(g) \rightarrow Fe_2O_3 + 2SO_2(g)$$

Complete regeneration has been achieved except at conditions of high pressure and low temperature. At these conditions small amounts of $Fe_2(SO_4)_3$ are apparently formed. Thermodynamic analysis using the free energy minimization program CHEMQ confirms that sulfate formation may occur at these conditions.

In steam, the desired regeneration reaction is

$$3FeS(s) + 4H_2O(g) \rightarrow Fe_3O_4(s) + 3H_2S(g) + H_2(g)$$

Only atmospheric pressure tests using steam have been completed and complete regeneration has been achieved. However, trace quantities of O_2 remaining in the reactor feed gas cause the subsequent oxidation of Fe_3O_4 to Fe_2O_3. This O_2 is believed to enter the electrobalance housing when the hangdown tube is removed for solid sample addition and removal. Dead spaces within the housing prevent complete O_2 removal by purging. However, the residual O_2 concentration

is believed to be sufficiently small (only a few ppm) that it has no significant effect on the rate of the reaction with steam until essentially all of the FeS has reacted.

The electrobalance studies show that the initial reaction rate is at most a weak function of temperature and gas flow rate, but a strong function of reactive gas mol fraction. Although the presently available data is limited, it appears that at a fixed temperature and reactive gas mol fraction, an increase in pressure from 1 to 5 atm produces a small increase in reaction rate while a further increase to 15 atm causes the rate to decrease.

GAS ANALYSIS

Both the Antek UV-fluorescence analyzer to be used to determine of total sulfur in the regeneration product gas, and parts needed to modify the Shimadzu GC-14A gas chromatograph to be used for H_2S and SO_2 analysis arrived early in the quarter. Problems during installation and calibration were encountered with both units. By the end of the quarter we feel that GC is working properly but problems remain with the Antek instrument.

Antek Total Sulfur Analyzer

A simplified flow diagram of the Antek unit is shown in Figure 1. A portion of the regenerator product gas enters the pyrolysis tube. The flow rate is controlled strictly by a capillary quartz flow restrictor which reduces the pressure of the gas from the reactor pressure to atmospheric. Excess oxygen is added to the pyrolysis tube and, at the operating temperature of 1050°C, all sulfur compounds are oxidized to SO_2. The oxidized product flows from the pyrotube through a membrane dryer for H_2O removal and then to the UV fluorescence sulfur detector.

Problems with an improper o-ring immediately downstream of the pyrolysis tube were encountered during the initial installation and testing. A low-temperature, non sulfur-resistant o-ring was installed where a high temperature, sulfur resistant Kalrez o-ring should have been used. A small H_2S leak, consisting only of the H_2S inventory in the 1/8-inch tubing leading from the H_2S cylinder to the instrument, resulted. However, this was sufficient to create quite an odor and resulted in the local fire department and hazardous materials unit being called. No damage resulted.

The o-ring was replaced with Kalrez and the unit provided the proper qualitative response during the second round of tests. However, small amounts of H_2SO_4 were formed in the high temperature oxidizing atmosphere of the pyrotube. The H_2SO_4 subsequently condensed downstream over a period of time. This time Antek supplied a small glass cyclone to be installed just downstream of the pyrotube. The cyclone has apparently collected most of the aerosol acid and we have subsequently been able to operate the unit without acid condensation.

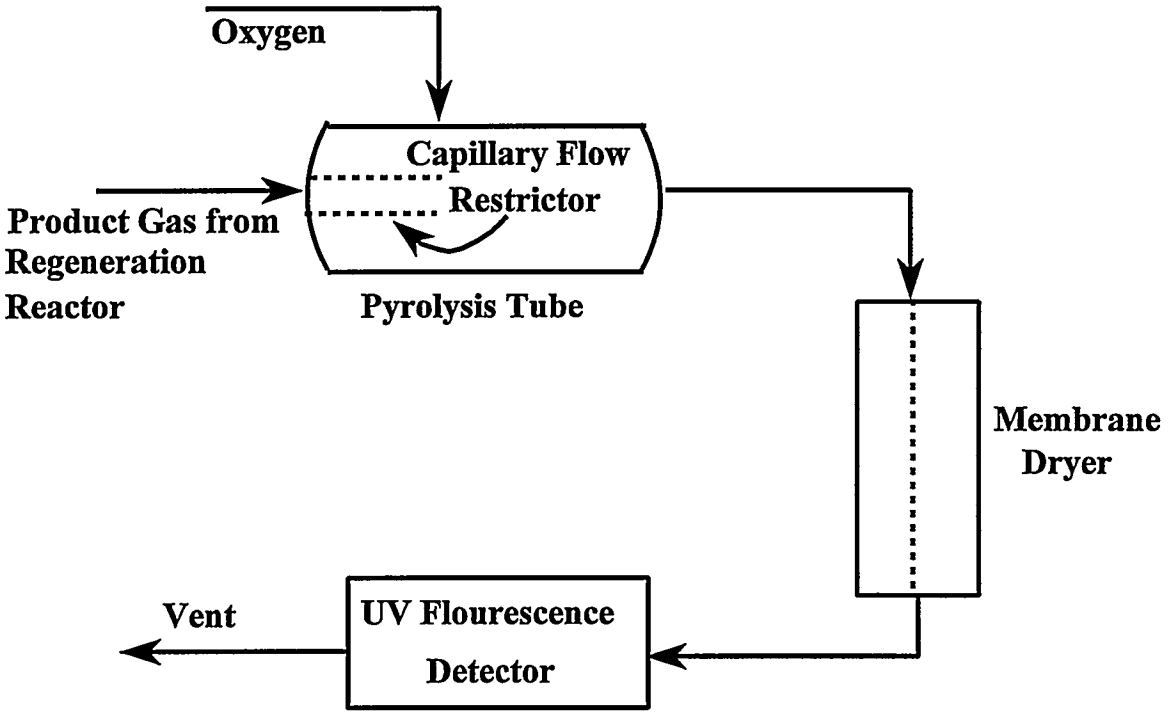

Figure 1. Simplified Diagram of the Antek Total Sulfur Analyzer

The volumetric flow rate of gas through the capillary restrictor at 1050°C is determined by the pressure upstream of the restrictor. A flow rate-pressure curve for N_2 at 1050°C was determined so that the flow rate could be quantified. Only minor differences between the flow rate of N_2 and the reactor product gas are expected. Results of this calibration are shown in Figure 2. At 225 psig, which is approximately the maximum pressure anticipated in the experimental tests, the flow rate is about 270 sccm. The flow rate decreases to about 25 sccm at 40 psig.

Sulfur calibration tests were then initiated by feeding known concentrations of H_2S in N_2 to the pyrotube and measuring the output from the analyzer. H_2S and N_2 flow rates were based upon the mass flow controller settings. Results of the first calibration test are shown in Figure 3. The total flow rate was 180 sccm, and the H_2S content ranged from 0 to 4.3%. The unit was first zeroed under pure N_2. 1.1% H_2S in N_2 was then added and the gain, sensitivity, and span were adjusted to provide an instrument reading of 110. H_2S content was then adjusted to provide from 0.23% to 4.31 % H_2S and the instrument reading was recorded. The numbers beside the data points in Figure 3 represent the sequence in which the data was taken.

A maximum in the instrument response is present at about 1% H_2S. This is unsatisfactory since two sulfur concentrations will produce the same instrument response. For example, an instrument reading of 80 could correspond to either 0.51% or 1.95% H_2S.

Reducing the total flow rate through the pyrolyzer shifted the maximum in the instrument response to higher H_2S concentrations. An example is shown in Figure 4 where total gas flow rate was reduced to 25 sccm by lowering the pyrotube inlet pressure. The maximum in the response curve was shifted to 5.7% H_2S, but instrument readings below the maximum could still correspond to two different concentrations. It is interesting to note that the maximum in Figure 3 corresponded to a H_2S flow rate of 1.8 sccm while the maximum in Figure 4 corresponded to 1.42 sccm H_2S. Given the uncertainty in identifying the exact maximum, particularly in Figure 3, it is possible that these two number are effectively the same.

It appears that the UV-fluorescence analyzer is becoming saturated by the high sulfur loadings. We are presently in contact with Antek about reducing the flow to the detector either by increasing the resistance of the capillary flow restrictor or by splitting the flow of gas from the pyrotube so that only a fraction of the total flow is fed to the detector. A third option may be to dilute the feed to the UV-analyzer by adding a known amount of inert gas downstream of the pyrotube.

Gas Chromatograph

When the Shimadzu representative first arrived to complete the instrument modifications, he found that no installation instructions had been included. Instructions were forwarded and a second visit was required to complete the installation. The GC will use two sampling valves and dual columns to accomplish the H_2S and SO_2 analysis and prevent interference from trace quantities of water vapor which might escape the condenser. The purpose of the first column

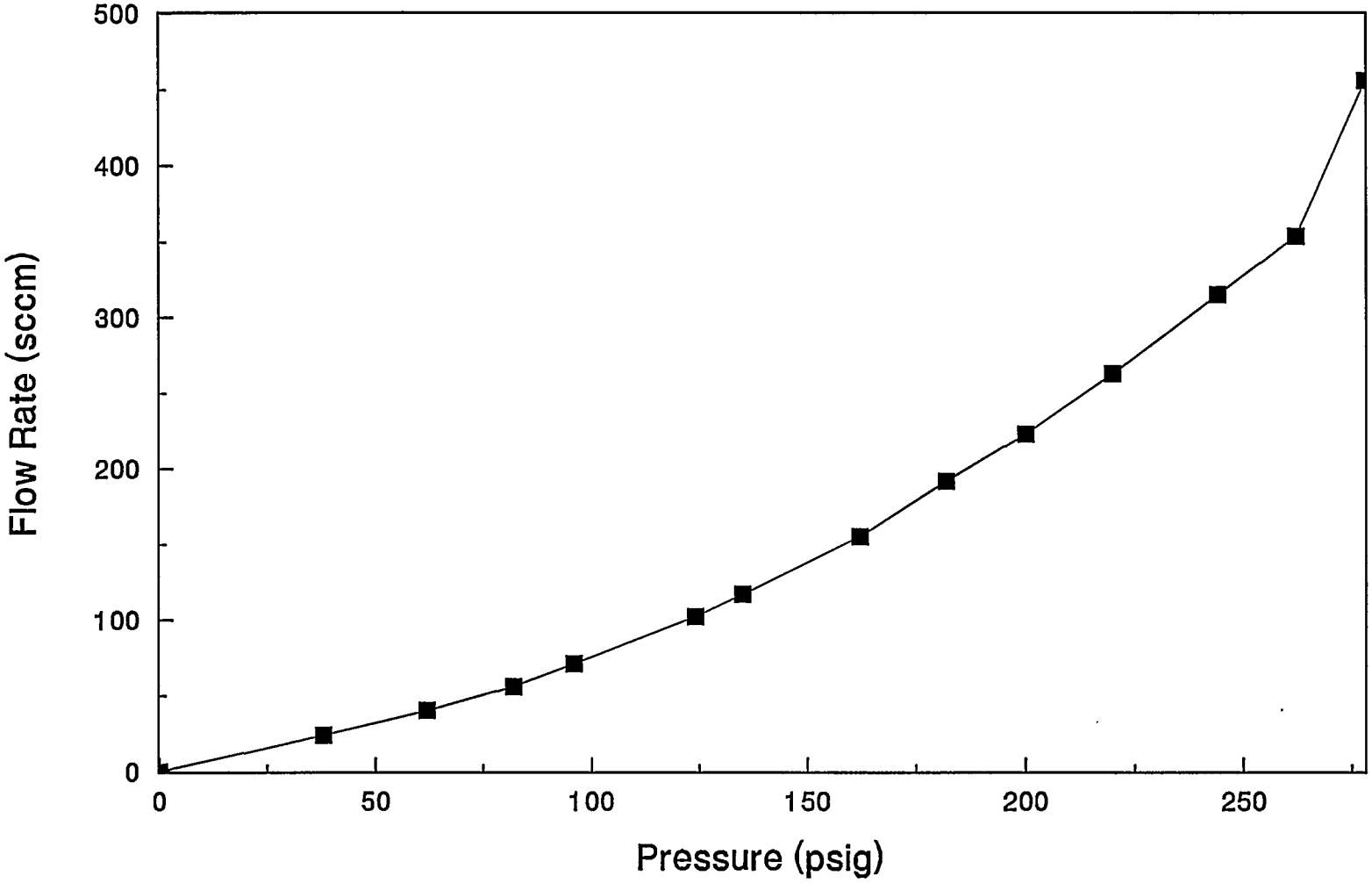

Figure 2. Pressure-Flow Rate Calibration Curve for the Antek Analyzer

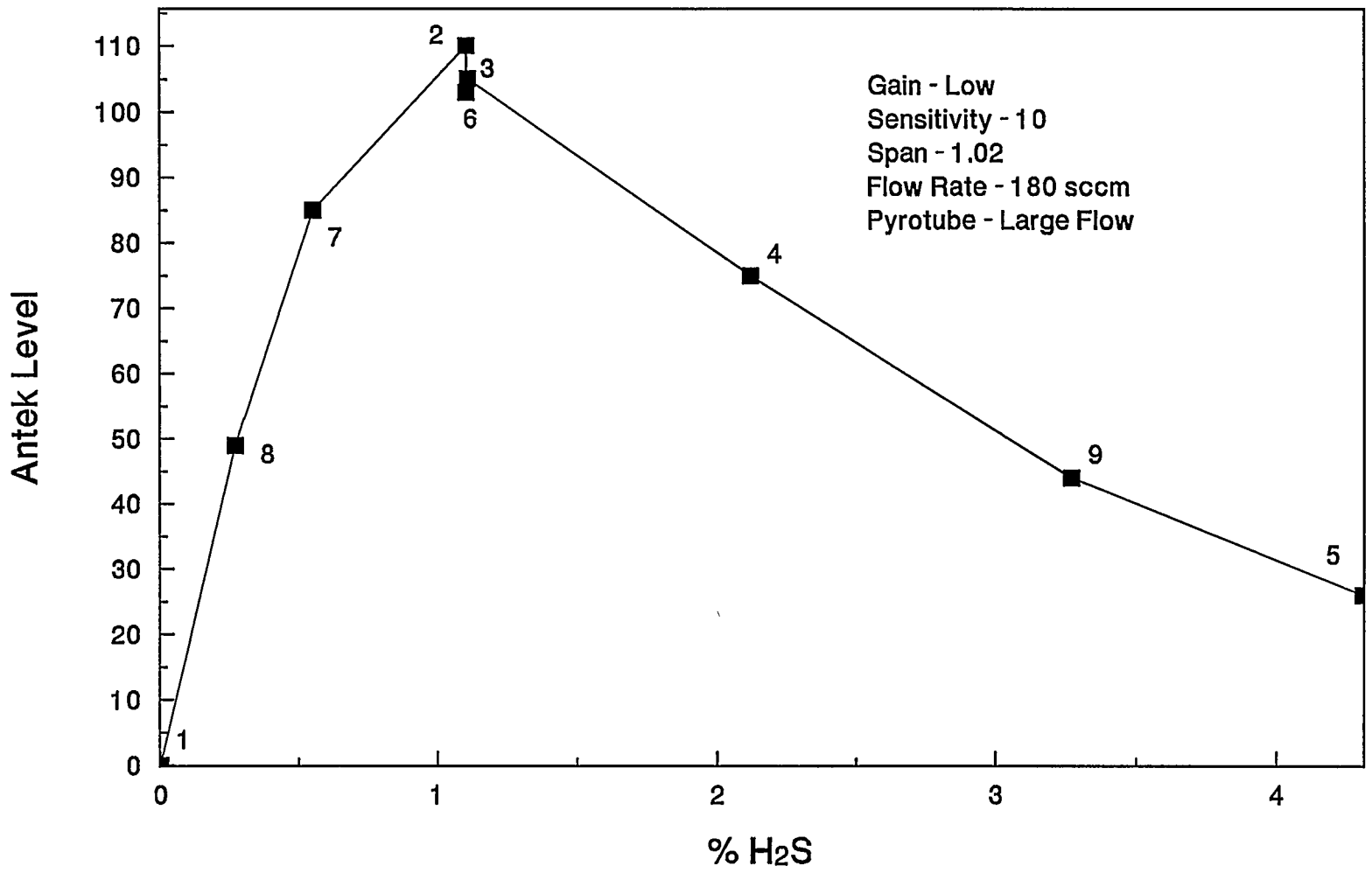

Figure 3. Results of the Initial Calibration Test of the Antek Total Sulfur Analyzer

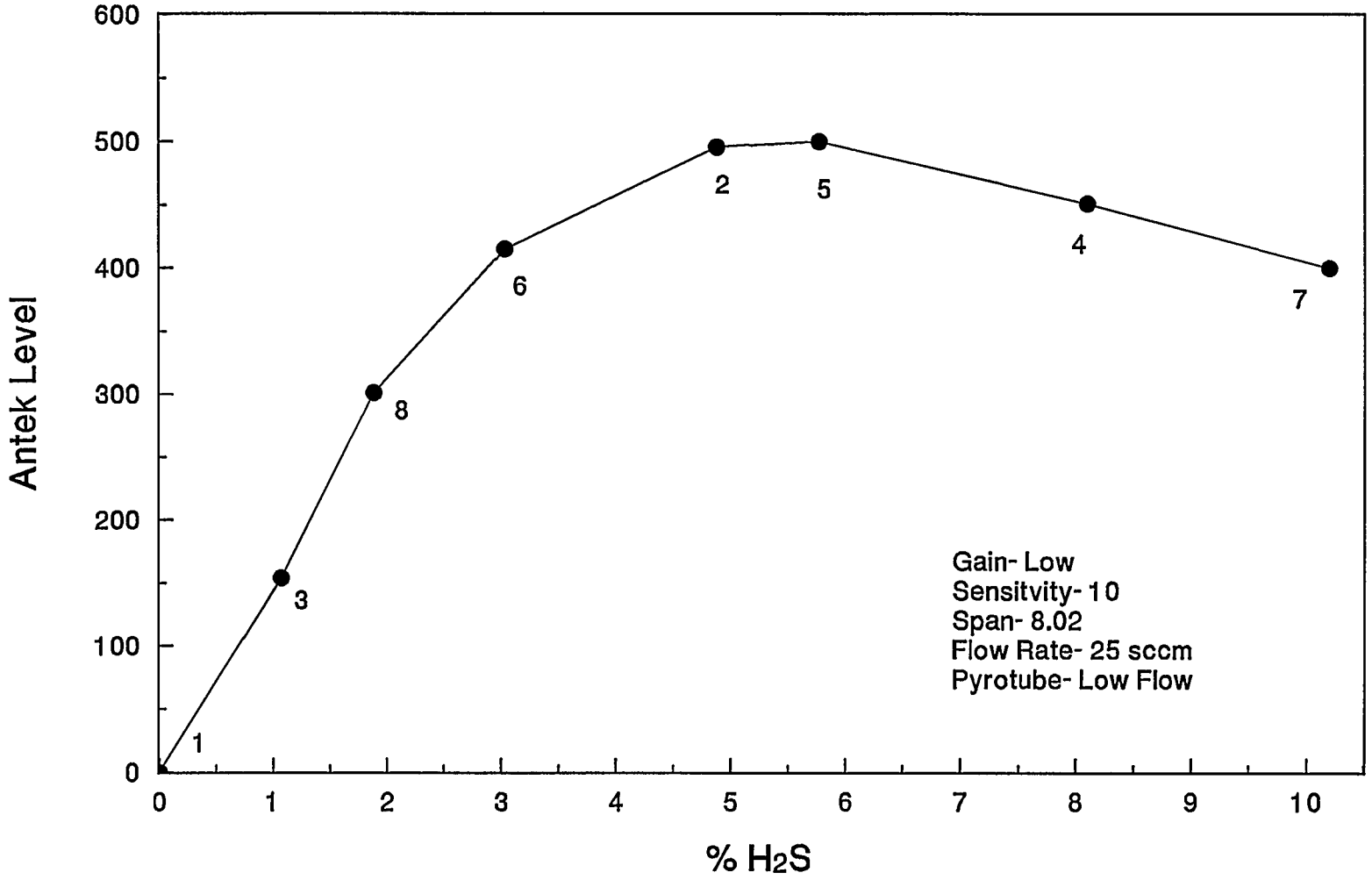

Figure 4. Calibration of the Antek Total Sulfur Analyzer Using a Total Gas Flow of 25 sccm

is to retain water while passing H_2S and SO_2. H_2S and SO_2 separation are achieved in the second column, and during this period water is flushed from the first column by a backflow of carrier gas. Unfortunately, the HayeSep T column, which was supposed to retain water and pass SO_2 and H_2S, trapped SO_2 as well as H_2O. A HayeSep Q column, which passed both SO_2 and H_2S, was subsequently obtained and we were able to proceed with GC calibration.

A diagram of the current GC sampling system is shown in Figure 5, and an explanation of the sampling and analysis sequence follows. Manually operated four-port sampling valve VO is used to select either the reactor feed or product gas for analysis. In the Figure 5 orientation the product gas is to be analyzed while the sample from the side-arm of the reactor feed is directed to vent. The feed gas to the GC consists of that fraction of the reactor product not sent to the Antek total sulfur analyzer. A condenser and filter for removal of elemental sulfur and steam are installed in the GC feed line.

The GC feed flows from VO to the automatically-actuated ten-port sampling valve VI. In the step one configuration, the feed enters VI, flows through the sample loop, back into VI, and exits to vent. Carrier gas C1 enters V1 and exits through the chromosil 310 (CRS) column and the thermal conductivity detector (TCD). Carrier gas C2 enters VI, passes in back-flow through the Haye Sep Q column, and then to vent. In this orientation C2 is backflushing traces of water which may have escaped condensation. The continuous flow of product gas through the sample loop insures that samples directed to the GC represent the reactor conditions at that time.

Step two in Figure 5 represents the actual sampling period. Valve VI is automatically rotated to the new position where product gas enters VI and flows directly to vent. Carrier gas C1 transfers the sample to be analyzed to HSQ where water is retained and SO_2 and H_2S are eluted. SO_2 and H_2S flow with the carrier gas to CRS where the SO_2 and H_2S are separated. Effluent from the CRS then flows through the thermal conductivity detector for analysis. C2 enters VI, backflushes water from HSQ, and passes to vent.

After backflushing is complete, VI is rotated back to its original position as shown in step three. The flows are identical to those in step one, and the system is ready for the next sample. At the operating conditions currently planned, sampling can be accomplished every 4 or 4½ minutes.

A typical chromatogram obtained during GC calibration is shown in Figure 6. The feed gas consisted of 86.7% N_2, 4.4% H_2S,and 8.7% SO_2, with feed rates controlled by the mass flow controllers. GC operating conditions were as follows:

C1 and C2	-	Helium
Oven Temp.	-	90°C
Haye Sep Q Column	-	8 ft x 1/16 in OD stainless steel
Chromosil 310 Column	-	8 ft x 1/8 in OD teflon

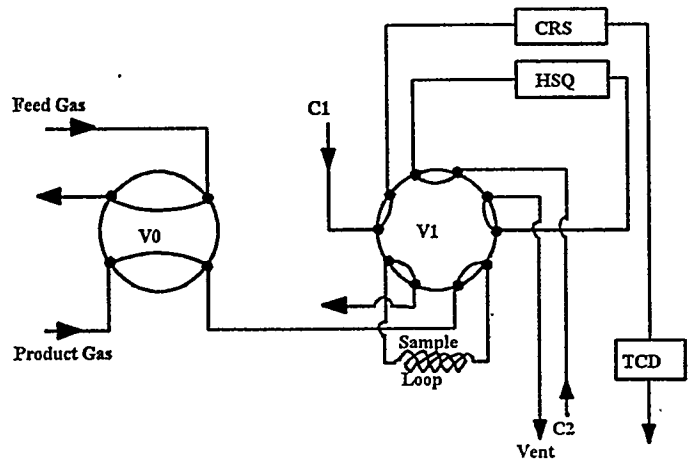

C1, C2: Carrier Gases
CRS: Chromosil 310 Column
HSQ: Hayesep Q Column
TCD: Thermal Conductivity Detector

GC Operation -- Step One

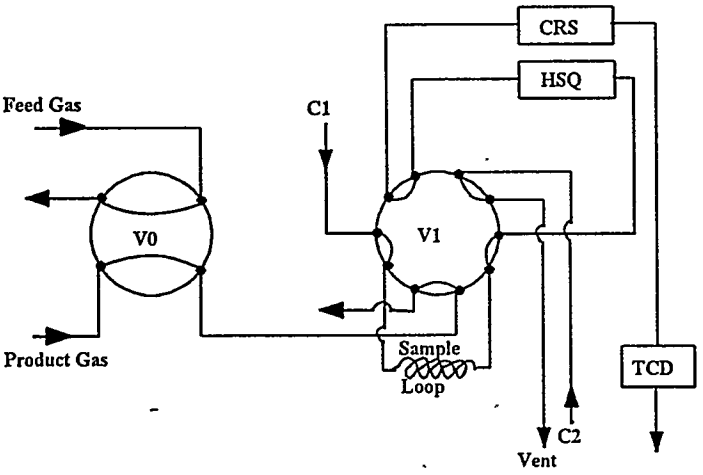

GC Operation -- Step Two

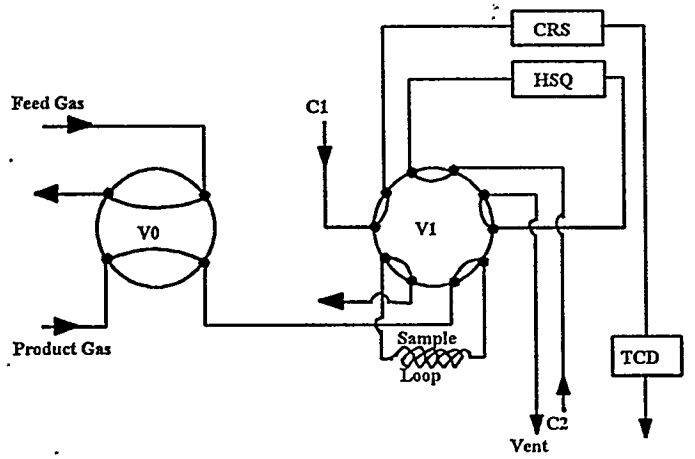

GC Operation -- Step Three

Figure 5. Schematic Diagram of the GC Sampling Sequence

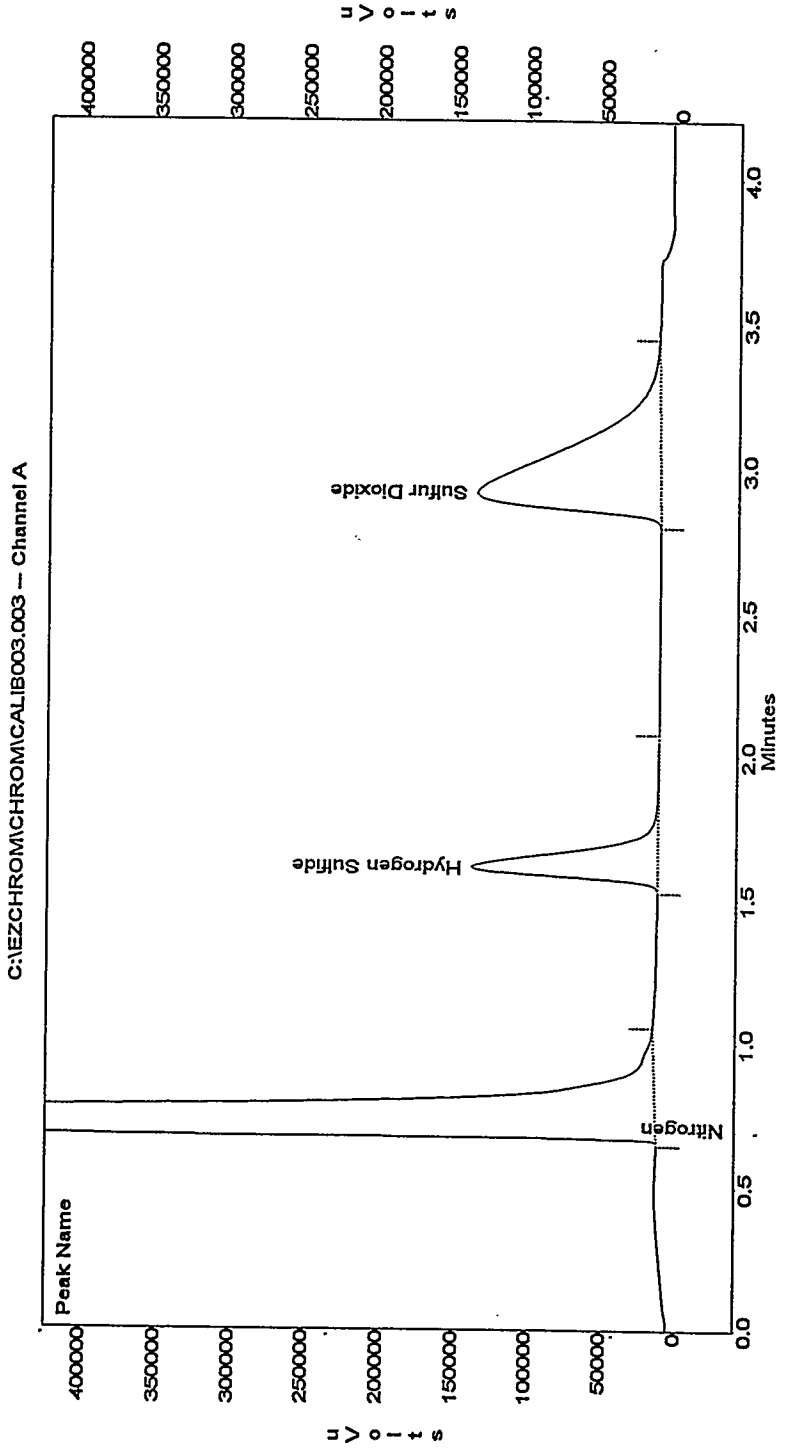

Figure 6. Typical Chromatogram Showing the Separation of H_2S and SO_2

Good component separation was achieved with retention times of 0.71 min for N_2, 1.61 min for H_2S, and 2.92 min for SO_2. The SO_2 retention time establishes the allowable sampling frequency.

Similar tests were conducted with other H_2S and SO_2 concentrations to establish the calibration curves shown in Figure 7. Linear regression of the results produced the following equations relating chromatogram area and mol percent:

$$\text{mol \% } H_2S = 6.174 \times 10^{-6} \text{ (Area } H_2S)$$
$$\text{Mol \% } SO_2 = 5.033 \times 10^{-6} \text{ (Area } SO_2)$$

Correlation coefficients for both compounds were greater than 0.999.

The minimum H_2S content of the calibration gas was 0.12% (1200 ppm), a limit which was established by the sensitivity of the mass flow controllers. The TCD analyzer, although not as sensitive for H_2S as other analyzers, should be capable of measuring H_2S concentrations somewhat below the lowest calibration level.

ELECTROBALANCE CHARACTERISTICS

Both an atmospheric pressure and high pressure electrobalance are being used to study the regeneration of FeS in atmospheres of O_2/H_2, H_2O/N_2, and $O_2/H_2O/N_2$. In the atmospheric pressure unit we are examining the effect of volumetric flow rate, temperature, and reactant gas mol fraction on the global kinetics of the regeneration reaction. The high pressure unit is being used to examine the above effects plus total pressure. At the present time we have looked at both O_2/N_2 and H_2O/N_2 atmospheres in the atmospheric pressure unit and only O_2/N_2 in the high pressure unit.

Aerodynamic Drag

The electrobalance measures the solid weight, which differs from the true solid mass when aerodynamic drag forces are important. The magnitude of the aerodynamic drag has been evaluated as a function of gas flow rate, temperature, and pressure by observing the apparent weight change in a nonreacting system when one of these parameters is changed.

There are two components to the aerodynamic drag. When the reaction temperature and pressure have reached their desired values, but before reactive gases are introduced, the solid reactant is exposed to inert gas flowing through the electrobalance housing at a rate Q_1 (vol/time), creating a drag D_1 (mg). Thus, the apparent weight at the beginning of the reaction is $W_o = M_o + D_1$, where M_o is the initial mass. Introduction of reactive gas by opening the valve in the electrobalance side-arm increases the volumetric flow rate to $Q_1 + Q_2$ and the effective drag to $D_1 + D_2$. D_2 cannot be determined under reaction conditions since the

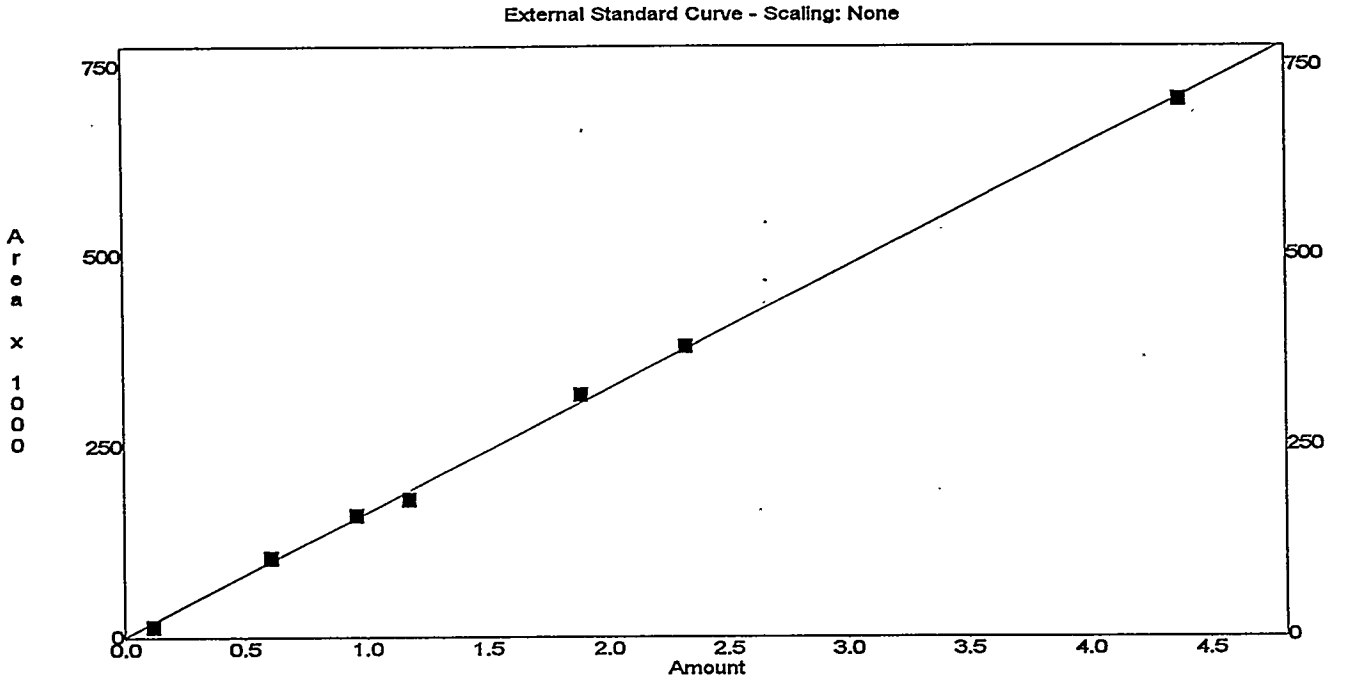

a) Hydrogen Sulfide

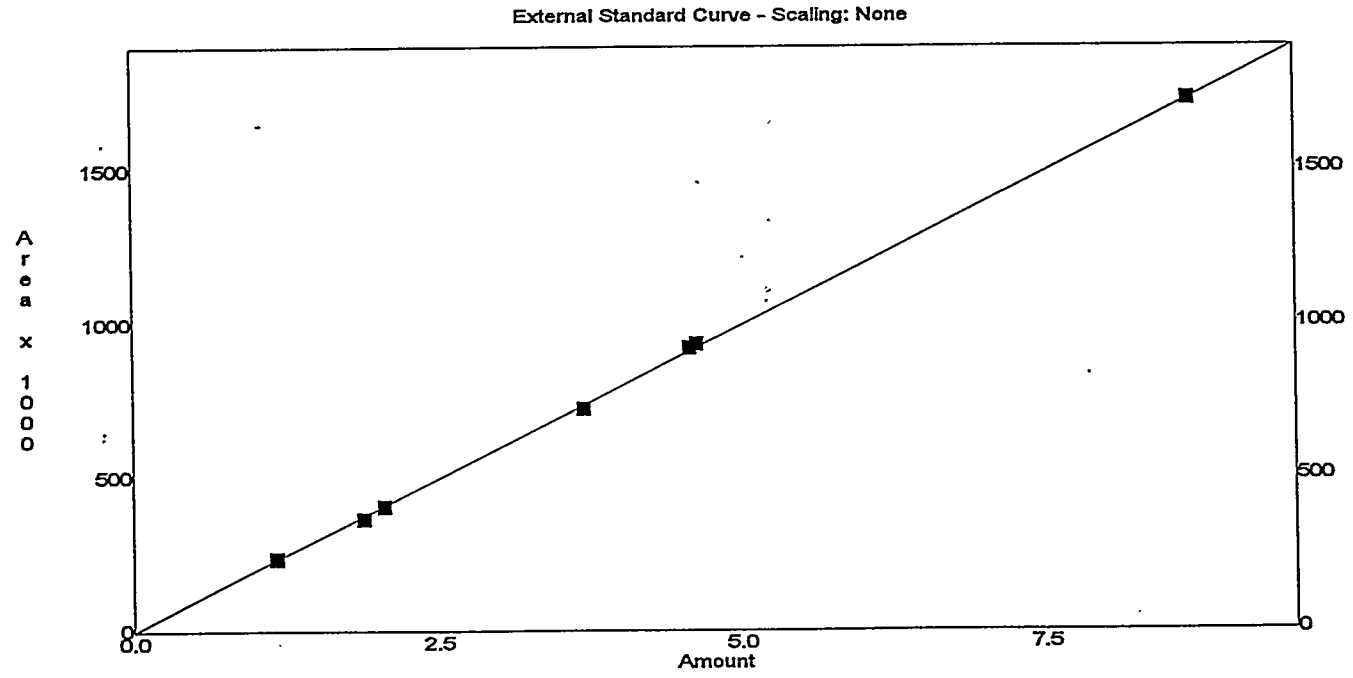

b) Sulfur Dioxide

Figure 7. H_2S and SO_2 Calibration Curves

regeneration reaction, which produces a decrease in solid mass, is initiated at the same time. After the reaction is complete the apparent weight is $W_f = M_f + D_1 + D_2$.

Figure 8 shows the magnitude of the aerodynamic drag under nonreacting conditions in the atmospheric pressure unit at 600°C. The drag was almost linear with flow rate for $Q < 300$ sccm, but increased at a slower rate at higher gas flow. Similar drag results from the high pressure electrobalance as a function of flow rate and pressure at a temperature of 700°C are shown in Figure 9. The drag was effectively linear in the range of flow rates studied and decreased with increasing pressure.

Knowledge of the magnitude of the aerodynamic drag allowed weight data from the two electrobalances to be converted to mass.

Delay Time

In each unit there is a time delay between opening the reactor side-arm valve to introduce reactive gases to the system and the sample being exposed to the full concentration of reactive gas. This time delay, which is a function of temperature, pressure, and volumetric flow rate, was estimated by assuming plug flow of gas through the volume between the side-arm valve and the position of the reacting solid. Although approximate, this approach appears to be adequate. All experimental time data reported in the remainder of this report have been corrected for the delay time.

Incomplete Regeneration

In all atmospheric pressure tests, complete regeneration of FeS to Fe_2O_3 in the O_2/N_2 atmosphere was achieved at all temperatures and O_2 mol fractions. However, in tests at high pressure and low temperature, the stable final mass of the solid was appreciably greater than that expected for Fe_2O_3. This was tentatively attributed to the formation of small amounts of $Fe_2(SO_4)_3$. Previous scoping tests at lower temperature had produced data which definitely suggested that $Fe_2(SO_4)_3$ was formed.

Thermodynamic equilibrium calculations using CHEMQ were carried out to confirm the possibility of $Fe_2(SO_4)_3$ being formed. Selected results are shown in Figure 10. In the region above and to the left of the line, complete regeneration of FeS to Fe_2O_3 is thermodynamically favored. Below and to the right of the line, the equilibrium solid consists of a mixture of Fe_2O_3 and $Fe_2(SO_4)_3$ in varying proportions. The position of the line is only approximate. The line shown corresponds to an initial gas atmosphere of 1% O_2/99% N_2 with a large ratio of gas to solid. Higher O_2 mol fractions cause a small upward shift in the line while lower O_2 mol fractions cause a downward shift. In addition, the exact position of the line is a weak function of the initial gas-to-solid molar ratio. Although the line shown in Figure 10 is approximate, the results generally agree with the experimental observations and provide additional evidence for the formation of $Fe_2(SO_4)_3$ at some conditions of interest.

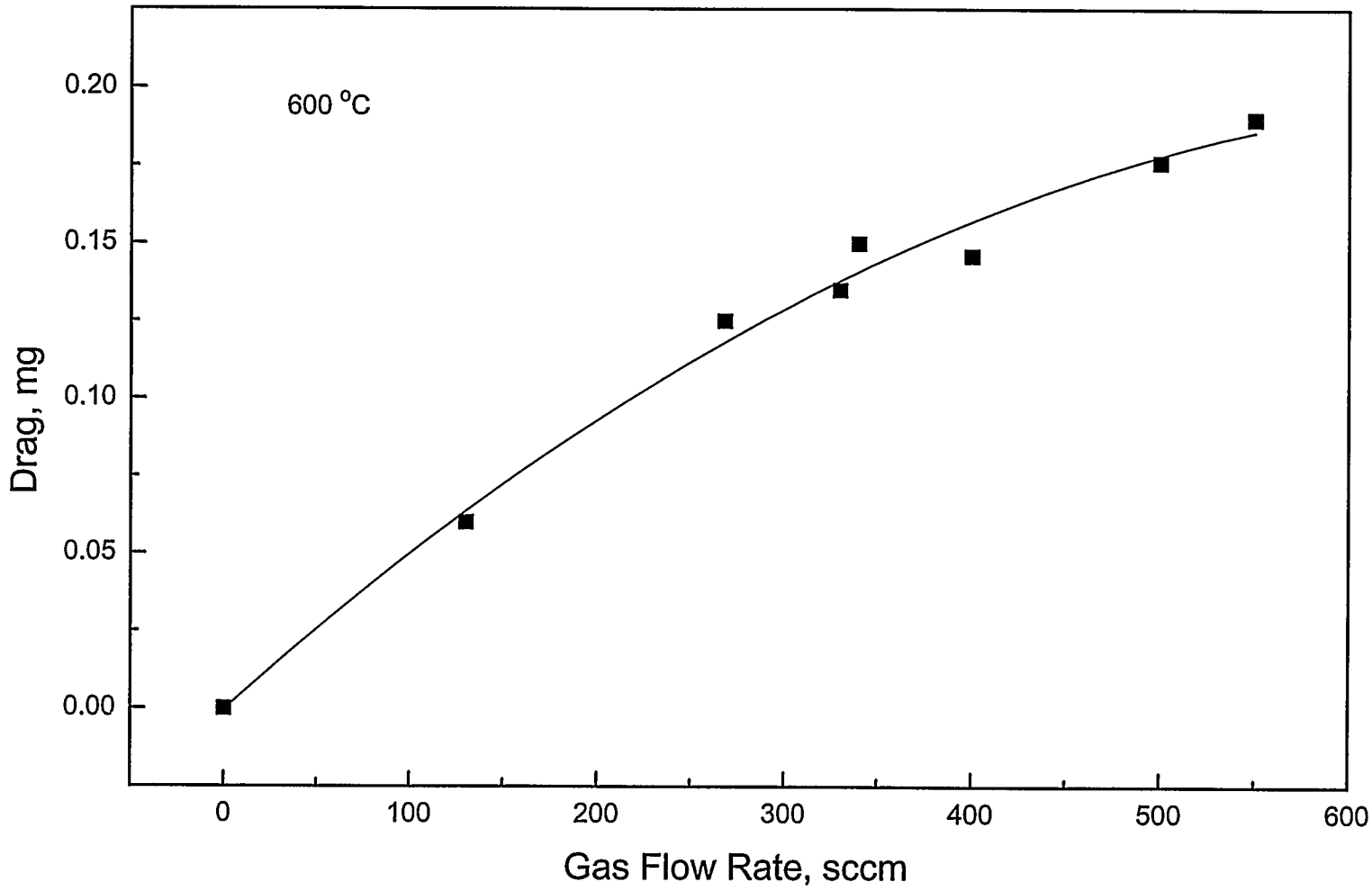

Figure 8. Aerodynamic Drag in the Atmospheric Pressure Electrobalance at 600°C

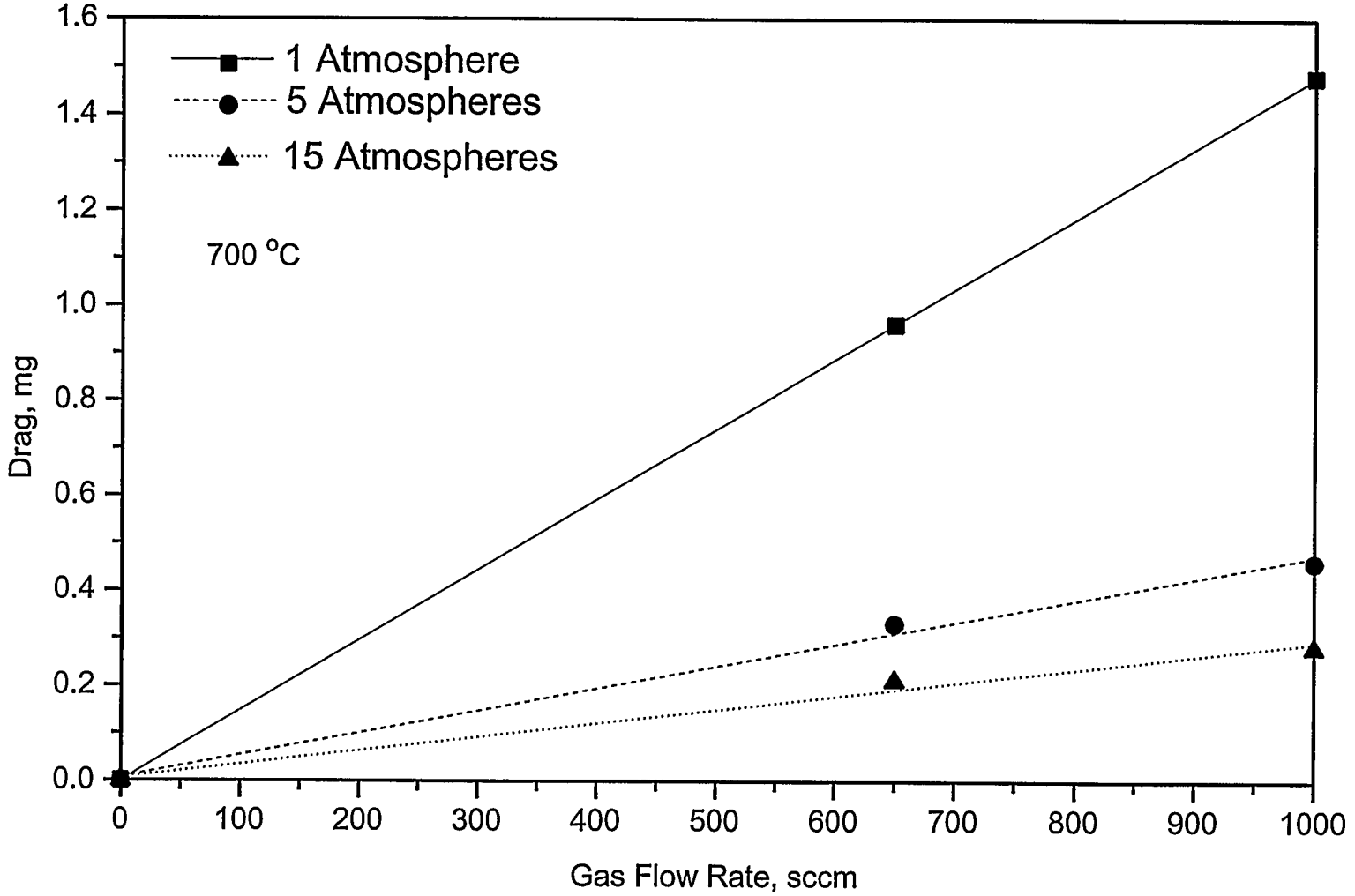

Figure 9. Aerodynamic Drag in the High Pressure Electrobalance at 700°C as a Function of Gas Flow Rate and Pressure

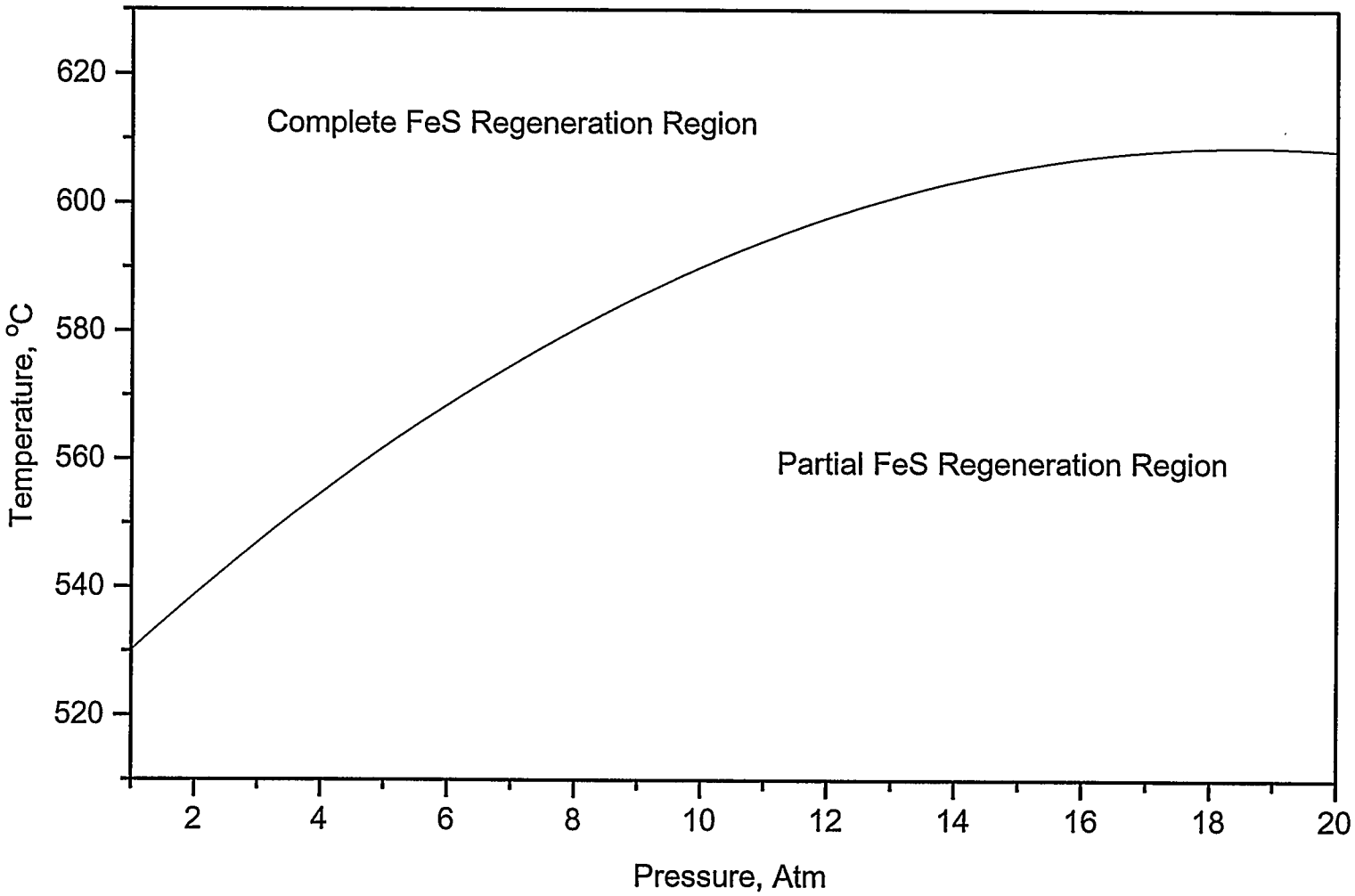

Figure 10. Thermodynamic Equilibrium Analysis for the Regeneration of FeS as a Function of Temperature and Pressure

For example, complete regeneration at 1 atm is predicted at all temperatures above about 530°C. The lowest temperature studied has been 550°C and complete regeneration was observed. Regeneration was incomplete at 600°C and 15 atm, and Figure 10 shows that a temperature somewhat greater than 600°C would be required to prevent completely the formation of $Fe_2(SO_4)_3$ at that pressure.

Typical Electrobalance Response Curves

After correction for the effects of aerodynamic drag and delay time, the electrobalance provides continuous data of sample mass as a function of time. For presentation purposes, we find it most convenient to report the mass ratio, M/M_o, as a function of time. This assists in the direct comparison of tests in which somewhat different values of M_o were used, and also establishes a target final value of M_f/M_o based on the stoichiometry of the reaction of interest. For the regeneration of FeS to Fe_2O_3 in the O_2/N_2 atmosphere, the theoretical value of M_f/M_o is 0.908. For the regeneration of FeS to Fe_3O_4 in the H_2O/N_2 atmosphere, the theoretical value of M_f/M_o is 0.876. Experimental values of the final mass ratio should obviously be reasonably close to the theoretical values.

A typical dimensionless mass-time curve for the regeneration of FeS in 3% O_2/N_2 at 800°C, 15 atm, and 650 sccm total gas flow is shown in Figure 11. Data have been manually smoothed to eliminate the electrobalance noise. The dimensionless mass decreases from its initial value of 1.0 and, in this case asymptotically approaches the theoretical final value of $M_f/M_o = 0.908$. The global reaction rate, which is proportional to the slope of the curve, is maximum at the beginning of the reaction and asymptotically approaches zero as the reaction approaches completion.

In most tests, the final value of M_f/M_o was somewhat less than the theoretical value. Possible reasons for this were discussed in the previous quarterly report. A complete report of values of M_f/M_o is presented in the tabular material of subsequent sections of this report.

A similar curve of dimensionless mass versus time for the regeneration of FeS in an atmosphere of H_2O/N_2 is presented in Figure 12. Reaction conditions for this test were 800°C, 1 atm, 20% H_2O/N_2, and 360 sccm gas flow rate. Once again the raw electrobalance data have been manually smoothed. In this example, the dimensionless mass decreased from its initial value of 1.0 and reached a minimum of 0.88 after about 30 minutes. Thereafter, the dimensionless mass increased and approached a final value of 0.908 after 110 minutes. The minimum dimensionless mass of 0.88 was just above the theoretical value of 0.876 for the complete conversion of FeS to Fe_3O_4, while the final value corresponded to the formation of Fe_2O_3. Similar results were observed in all tests using H_2O/N_2.

This behavior suggests the presence of small concentrations of O_2 in the H_2O/N_2 atmosphere. Because the ratio of H_2O to O_2 is quite high, initially the reaction between FeS and H_2O dominates. As the amount of FeS decreases and the amount of Fe_3O_4 increases, the

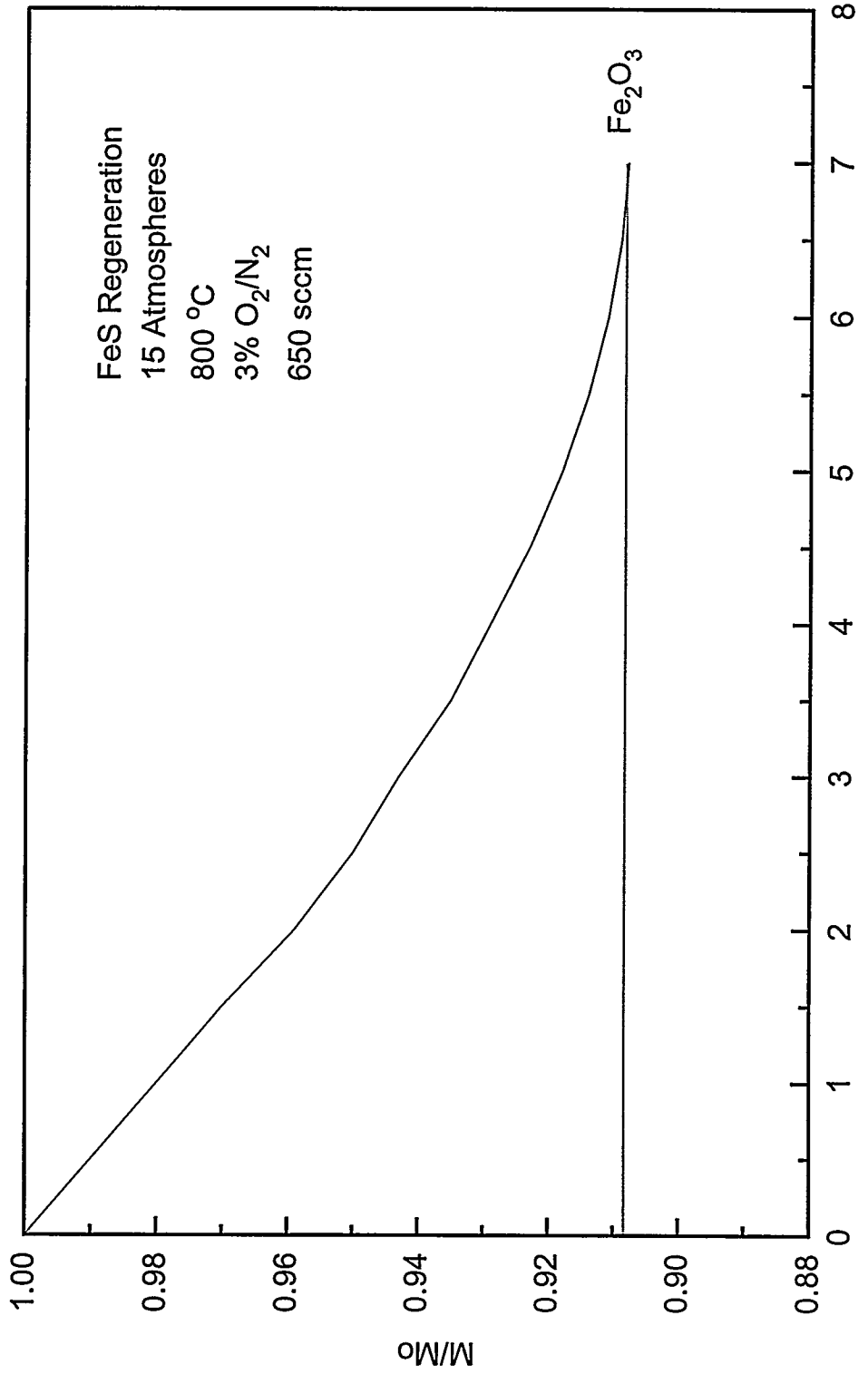

Figure 11. Dimensionless Mass Versus Time Response for the Regeneration of FeS to Fe_2O_3 in O_2/N_2

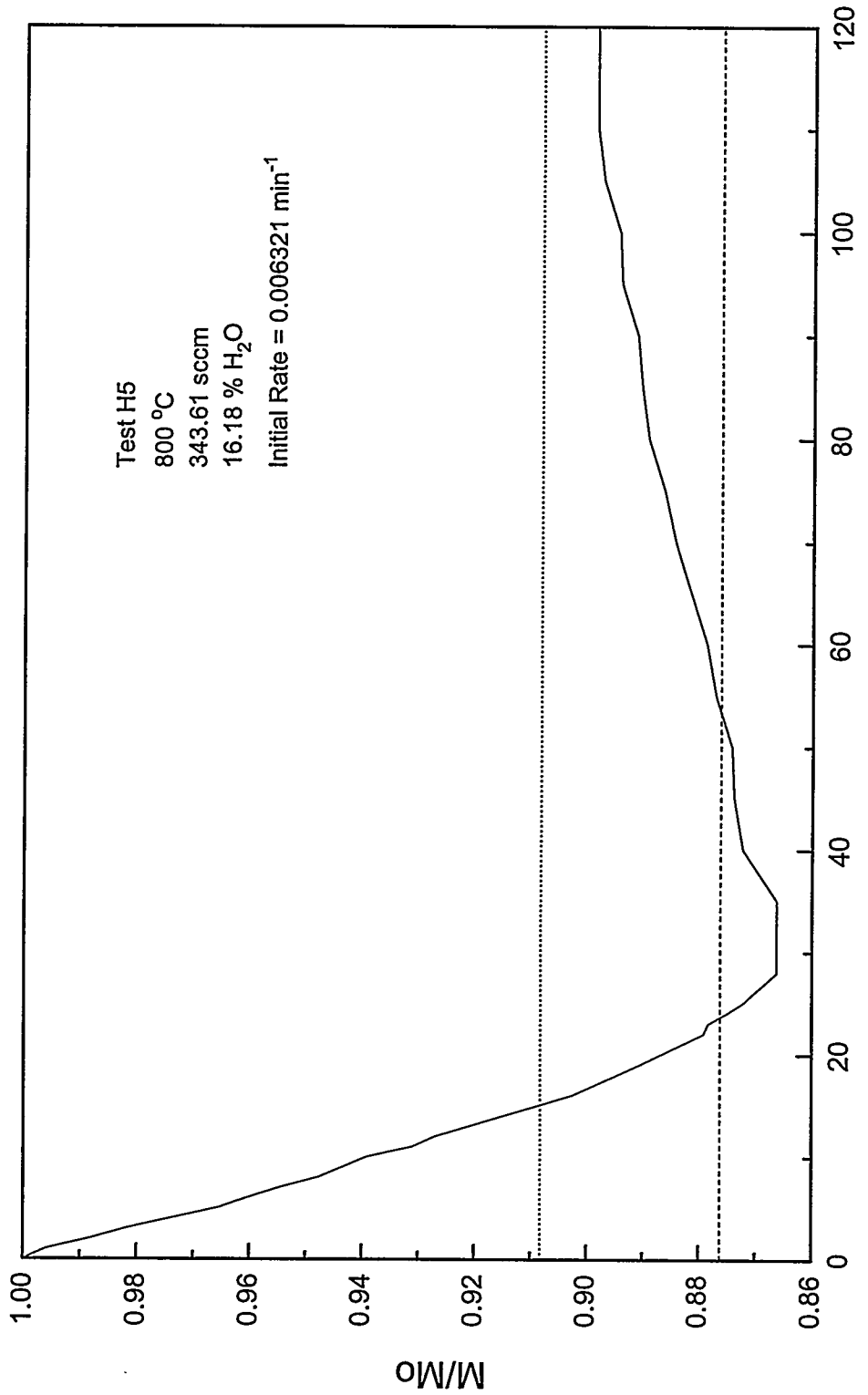

Figure 12. Typical Electrobalance Response for the Regeneration of FeS in H_2O/N_2

reaction of FeS with H_2O becomes less important and the oxidation of Fe_3O_4 to Fe_2O_3 becomes the dominant reaction.

Several attempts were made to identify and eliminate the source of the O_2. N_2 was bubbled through water used in the syringe pump to remove dissolved O_2. Ultra high purity N_2 having a maximum O_2 specification of 1 ppm was used. A trap capable of reducing the O_2 concentration to 0.1 ppm was added to the N_2 feed line. None of these changes made a significant difference in the electrobalance response curve. We now believe that O_2 is introduced into the electrobalance housing when the hangdown tube is removal for sample loading and unloading. A N_2 purge is maintained during this time, and continued after the hangdown tube is reattached. However, the purge is unlikely to eliminate totally back diffusion of air into the housing when the hangdown tube is removed, and the geometry of the housing is such that it is impossible to purge the unit completely. The residual O_2 concentration is believed to be sufficiently small (only a few ppm) to have a negligible effect on the reaction until the majority of FeS has been converted to Fe_3O_4.

Initial Reaction Rate

Inspection of Figures 11 and 12 indicates that the dimensionless mass-time curves are approximately linear for a reasonable period of time after the beginning of the reaction. The negative of the slope of the curve, $-d(M/M_o)/dt$, is proportional to the global reaction rate. We have estimated the initial slope and in the following sections this slope is reported as the initial reaction rate (units are min^{-1}). The effects of the reaction parameters -- temperature, pressure, flow rate, and O_2 mol fraction -- are then compared on the basis of the initial reaction rate.

ATMOSPHERIC PRESSURE ELECTROBALANCE RESULTS

The atmospheric pressure electrobalance has been used to study the regeneration of FeS in O_2/N_2 and H_2O/N_2 atmospheres. Although neither of these test sequences is complete at this point, sufficient data are available to obtain a general understanding of the qualitative effects of the reaction parameters -- temperature, gas flow rate, and O_2 or H_2O mol fraction.

Table 1 summarizes reaction conditions and key results for tests completed through September. The first block of data applies to the O_2/N_2 tests while the second block applies to the H_2O/N_2 tests. Columns 1 and 2 identify the date of the run and the run number. Columns 3, 4, and 5 establish the test conditions -- temperature, flow rate, and mol fraction of reactive gas. The initial solid mass is designated M_o and is found in column 6. This number is determined from the electrobalance at reaction temperature, and may differ slightly from the initial mass measured at ambient temperature if, for example, the ambient temperature sample contains adsorbed moisture. The initial mass varied between 2.1 and 2.72 mg. Column 7 displays the final solid mass in the case of the O_2/N_2 tests and the minimum solid mass in the case of the H_2O/N_2 tests. Column 8 is blank for the series of O_2/N_2 tests but shows the final mass for the H_2O/N_2 tests. Columns 9 and 10 are analogous to 7 and 8 except that the

Table 1. Summary of Reaction Conditions and Key Results from Atmospheric Pressure Electrobalance Tests

FeS Regeneration in O_2/N_2

Date	RUN	T	Qt	O2	Mo	M1	M2	(M1/Mo)	(M2/Mo)	rate
		C	sccm	%	(mg)	(mg)	(mg)	(mg)	(mg)	(min^-1)
28/6/95	B6	600	130	0.5	2.688		2.401		0.893	0.007
28/6/95	B7	600	130	1	2.729		2.426		0.889	0.0108
30/6/95	B10	600	130	3	2.6		2.316		0.891	0.0337
30/6/95	B11	600	130	3	2.55		2.27		0.89	0.0362
05/7/95	C2	600	260	3	2.353		2.098		0.891	0.044
07/7/95	C4	600	260	0.5	2.497		2.223		0.89	0.0072
07/7/95	C5	600	260	1	2.577		2.285		0.887	0.0152
10/7/95	C6	600	260	1	2.629		2.339		0.89	0.0135
12/7/95	D2	600	500	1	2.573		2.344		0.911	0.0155
13/7/95	D3	600	500	3	2.612		2.328		0.891	0.0458
14/7/95	D4	600	500	0.5	2.671		2.356		0.882	0.0075
17/7/95	E1	600	300	3	2.693		2.401		0.892	0.0331
18/7/95	E2	650	300	3	2.439		2.165		0.888	0.0386
19/7/95	E3	700	300	3	2.622		2.331		0.889	0.0496
20/7/95	E4	600	300	1	2.536		2.261		0.892	0.0116
24/7/95	E6	600	300	0.5	2.614		2.326		0.89	0.0077
25/7/95	E7	600	300	1	2.671		2.369		0.887	0.0114
26/7/95	E8	700	300	0.5	2.486		2.217		0.892	0.0077

FeS Regeneration in H_2O/N_2

Date	RUN	T	Qt	H2O	Mo	M1	M2	(M1/Mo)	(M2/Mo)	rate
		C	sccm	%	(mg)	(mg)	(mg)	(mg)	(mg)	(min^-1)
21/8/95	H2	800	286.4	0.162	2.374	2.069	2.159	0.872	0.909	0.0065
22/8/95	H3	800	286.4	0.162	2.339	2.039	2.109	0.872	0.902	0.0061
23/8/95	H4	800	343.6	0.162	2.426	2.146	2.206	0.885	0.909	0.006
24/8/95	H5	800	343.6	0.162	2.476	2.146	2.226	0.867	0.899	0.0063
25/8/95	H6	800	335.6	0.249	2.347	2.032	2.122	0.866	0.904	0.0092
20/9/95	H14	800	300	0.2	2.47	2.172	2.259	0.879	0.915	0.0083
21/9/95	H15	800	300	0.2	2.379	2.08	2.17	0.874	0.912	0.0084
23/9/95	H16	800	300	0.4	2.431	2.132	2.171	0.877	0.893	0.0134

dimensionless mass ratio, M/M_o is shown. Column 11 contains the estimate of the initial global reaction rate in units of min^{-1} which was obtained by estimating initial slopes. Note from column 9 of the O_2/N_2 block that the ratio is, with one exception, smaller than the theoretical value of 0.908. The column 9 entries for the H_2O/N_2 block are all within ± 0.010 mg of theoretical. It is possible that some of the values in columns 8 and 10 of the H_2O/N_2 block do not represent true steady states. The rate of conversion of Fe_3O_4 to Fe_2O_3 was so small near the end that some tests may have been terminated before true completion.

Reproducibility

The reproducibility of the initial reaction rate is of concern since its estimation requires that aerodynamic drag and time delay corrections be made, that the electrobalance response be properly smoothed to eliminate noise, and that the initial slope of the M/M_o versus time curve be properly evaluated. Duplicate tests at six sets of reaction conditions are available, and results are summarized in Table 2. The important entry in this table is in the last column where the maximum percent variation between the rate of an individual test and the average rate of all tests at the same reaction conditions are compared. The values range from 0% to 6.2%, which is surprisingly good considering all of the uncertainties involved in estimating the initial rate. Additional reproducibility runs will be carried out as the test program proceeds. We hope to be able to assign confidence limits to the initial rates.

Gas Flow Rate

In initial O_2/N_2 tests the gas volumetric flow rate was varied over a range of 130 to 500 sccm. As shown in Figure 13, the initial rate was only a weak function of flow rate. Consequently, in most of the subsequent tests the volumetric flow rate was standardized at 300 sccm. The same standard volumetric rate of 300 sccm was selected for the H_2O/N_2 test series. However, an error in the syringe pump setting in early H_2O/N_2 tests produced the unintended variation between 286 and 336 sccm which is shown in Table 1.

Temperature

The effect of temperature in a series of O_2/N_2 regeneration tests at 300 sccm and 3% O_2 is shown in Figure 14. A best-fit straight line is drawn through the three data points although there is no theoretical basis for a straight line response. The important observation from Figure 14 is that the initial rate only increased from 0.0331 min^{-1} at 600°C to 0.0496 at 700°C, which corresponds to an activation energy of about 6500 cal/mol. This relatively small temperature dependence suggests that transport resistances instead of surface reaction control the global rate. All H_2O/N_2 regeneration tests shown in Table 1 were at 800°C so that no analysis of the magnitude of the temperature effect is possible at this time. However, because the global rates for the H_2O/N_2 are much smaller, we expect to see a stronger temperature effect.

Table 2. Reproducibility of the Initial Reaction Rate from Multiple Tests at the Same Reaction Conditions

Temp., °C	Flow Rate, sccm	Mol Fraction	Test No.	Initial Rate, min^{-1}	Avg. Initial Rate, min^{-1}	Percent Variation
O_2/N_2 Tests						
600	130	0.03	B10	.0337	0.0350	3.7
			B11	.0362		
600	130	0.01	C5	.0152	0.0144	6.2
			C6	.0135		
600	300	0.01	E4	.0116	0.0115	0.9
			E7	.0114		
H_2O/N_2 Tests						
800	286	0.162	H2	.0065	0.0063	3.2
			H3	.0061		
800	344	0.162	H4	.0060	0.0062	3.3
			H5	.0063		
800	300	0.200	H14	.0083	0.0083	0
			H15	.0083		

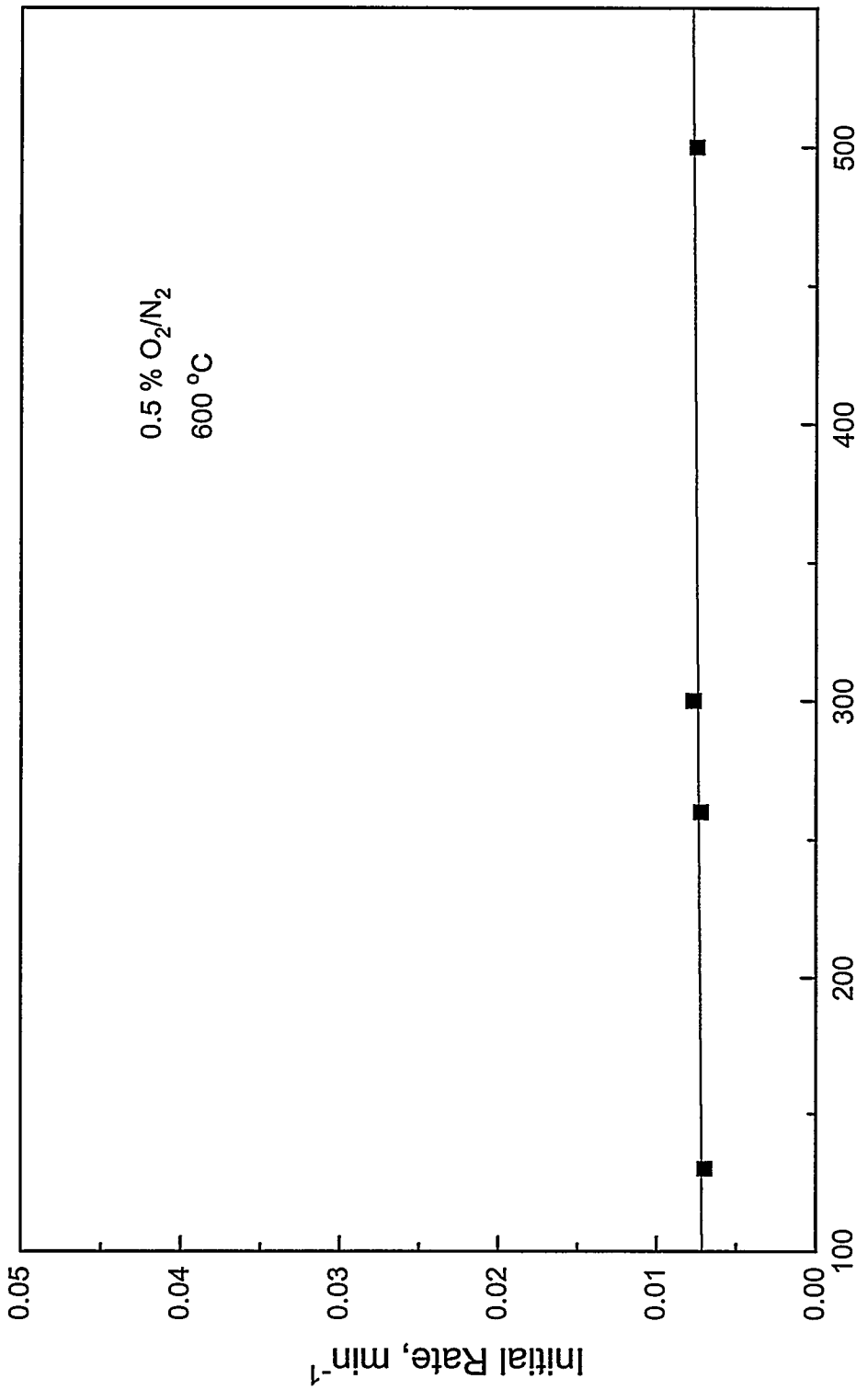

Figure 13. The Effect of Volumetric Gas Flow Rate on the Initial Reaction Rate for the Regeneration of FeS in O_2/N_2

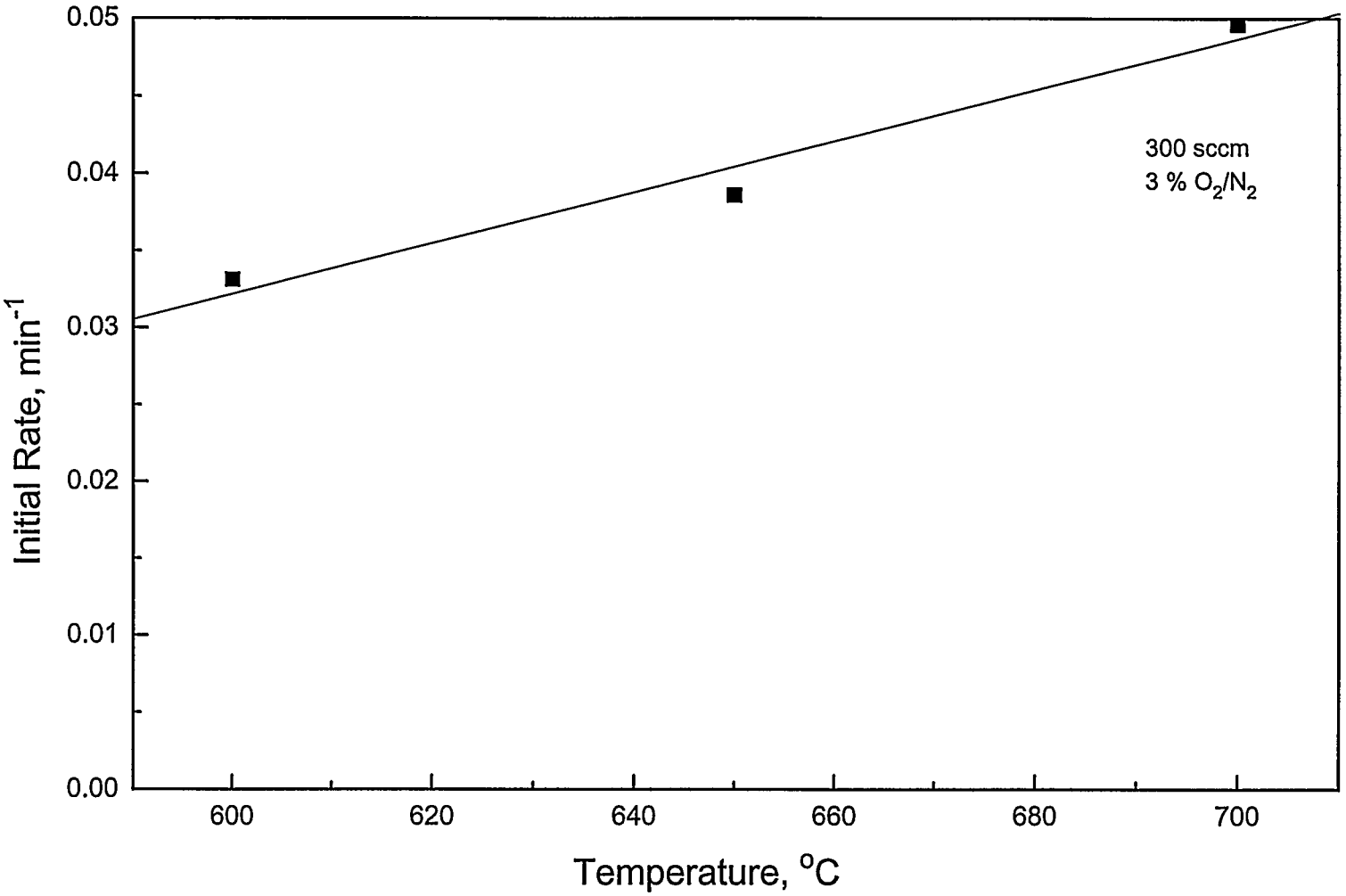

Figure 14. The Effect of Temperature on the Initial Regeneration Rate of FeS in O_2/N_2

Mol Fraction Reactive Gas

Reactive gas concentration has a major effect on the initial reaction rate in both the O_2/N_2 and the H_2O/N_2 reactions as shown in Figures 15 and 16, respectively. The O_2/N_2 data in Figure 15 is from a series of tests at 600°C and 300 sccm with the O_2 mol fraction varying from 0.005 to 0.03. Reaction conditions for the H_2O/N_2 system shown in Figure 16 are 800°C, 300 sccm. The H_2O mol fraction, which varied from 0.16 to 0.5, was considerably larger. The lines in both figures are reasonably straight, confirming that the global rate is first-order in both O_2 and N_2. The slope of the lines is equal to the first-order rate constant. Thus for O_2 at 600°C, the data is consistent with the following rate equation

$$\frac{-d\ (M/M_o)}{dt} = 1.12\ min^{-1}\ y_{o_2}$$

For H_2O at 800°C, the corresponding rate equation is

$$\frac{-d\ (M/M_o)}{dt} = 0.036\ min^{-1}\ y_{H_2O}$$

These equations confirm that the regeneration reaction is much faster in O_2 than H_2O.

HIGH PRESSURE ELECTROBALANCE RESULTS

To date, high pressure electrobalance tests have been limited to the regeneration of FeS in an O_2/N_2 atmosphere. Reaction parameters being investigated are temperature, gas flow rate, O_2 mol fraction, and pressure. We had hoped to complete the O_2/N_2 test series by the end of the quarter, but equipment problems were encountered beginning near the middle of September. Although the test sequence is incomplete, sufficient data is available to evaluate the effects of the reaction parameters, and, for appropriate tests, to compare results from the two electrobalance reactors.

Table 3 summarizes reaction conditions and key results for all "good" tests involving the regeneration of FeS in O_2/N_2 completed by the end of the quarter. The columns in Table 3 correspond to the columns of Table 1. There are eight complete data sets showing the effect of O_2 mol fraction, temperature, and pressure on the initial rate.

With two exceptions, the ratio of final to initial mass (M_f/M_o) of the runs in Table 3 were between 0.895 and 0.912, reasonably close to the theoretical value of 0.908. In general, the agreement with theory was better in the high pressure electrobalance than the low pressure unit. The two tests in which the M_f/M_o ratio was substantially higher than expected were run at 15 atm and 600°C, conditions where $Fe_2(SO_4)_3$ formation is favored. The amount of sulfate formed

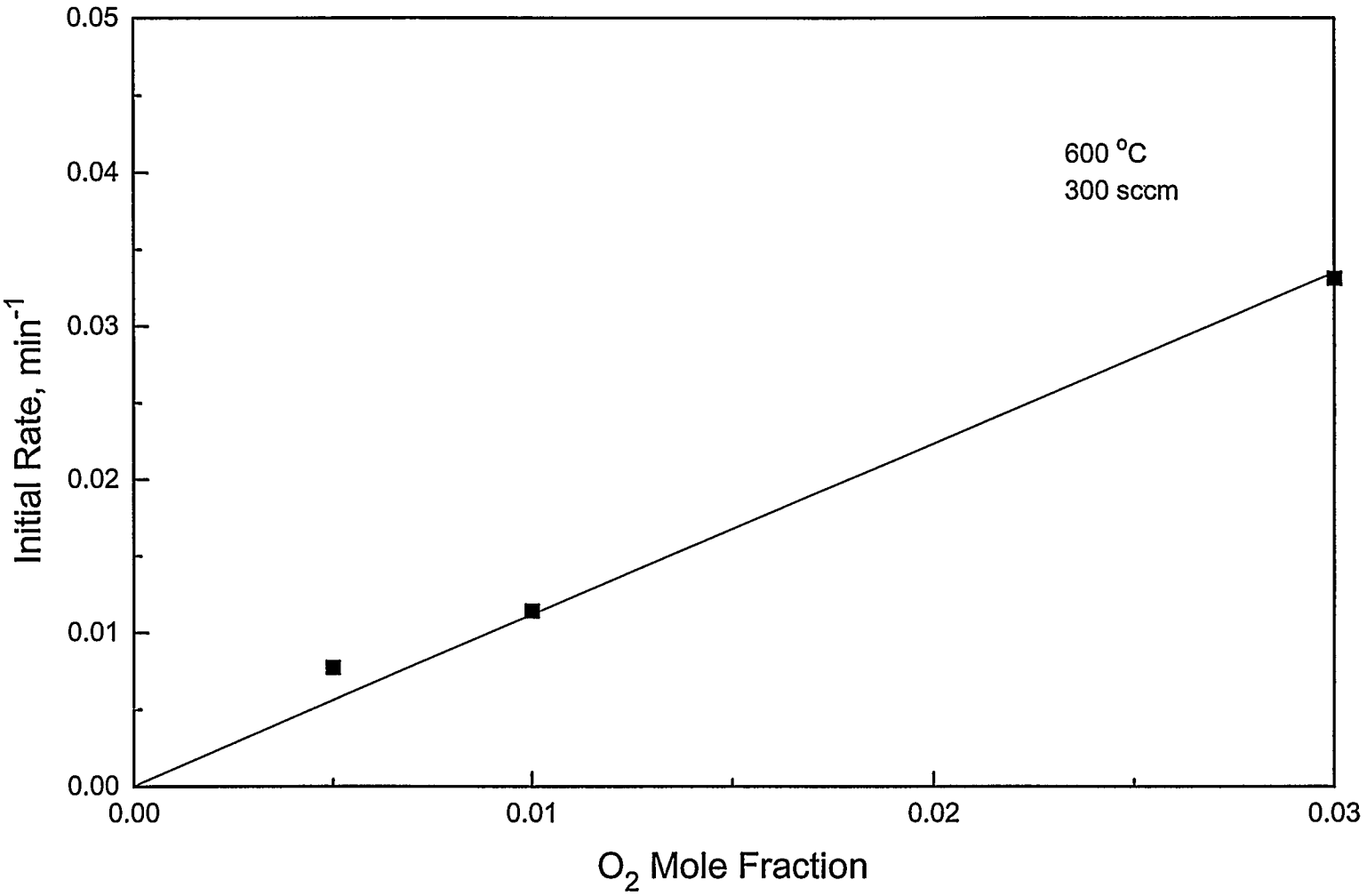

Figure 15. The Effect of O_2 Mol Fraction on the Initial FeS Regeneration Rate

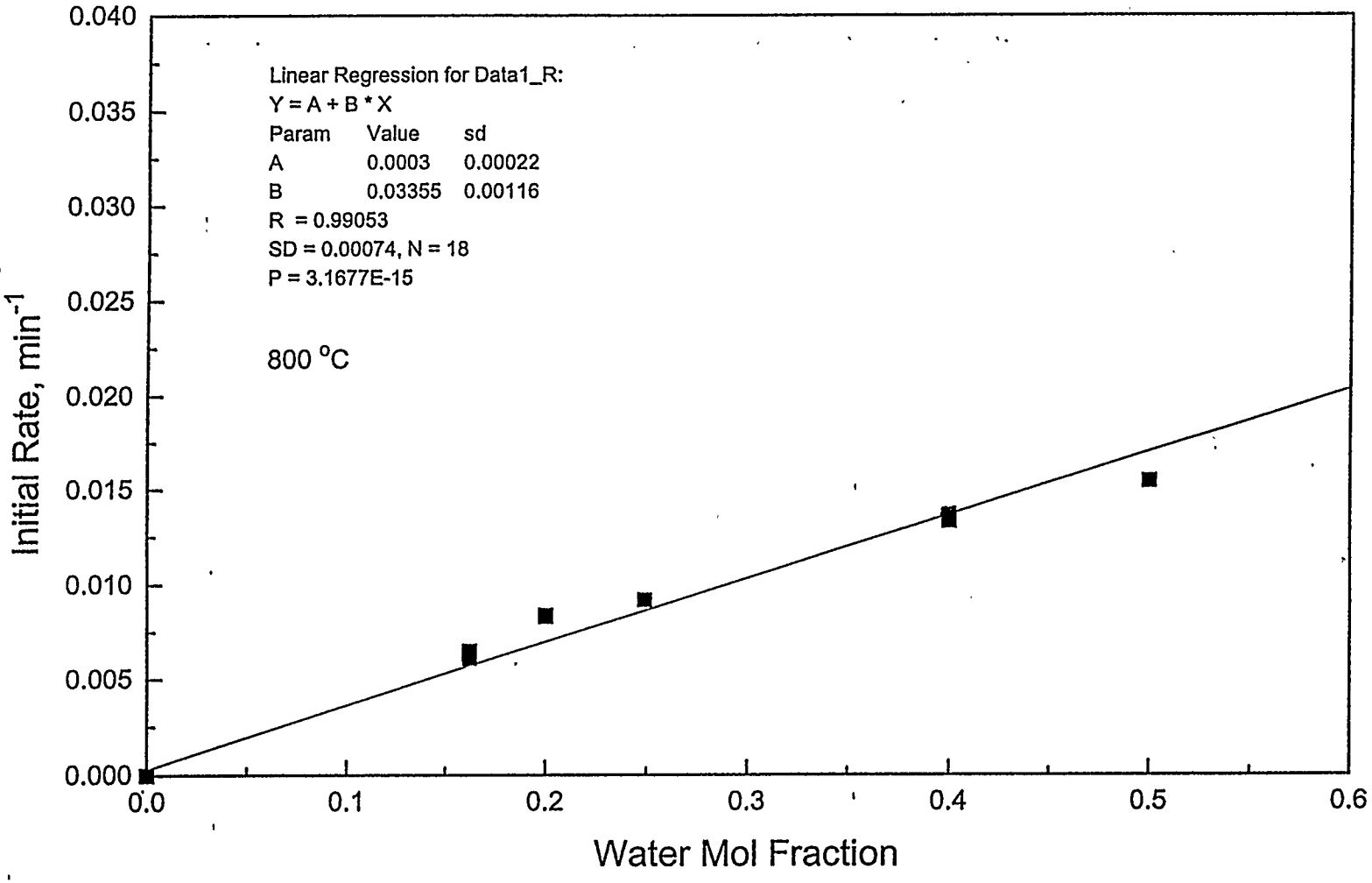

Figure 16. The Effect of H_2O mol Fraction on the Initial FeS Regeneration Rate

Table 3. Summary of Reaction Conditions and Key Results for the Regeneration of FeS in the High Pressure Reactor

FeS Regeneration in O_2/N_2

Date	Run	T (C)	Q (sccm)	Composition	P (atm)	Mo (mg)	Mf (mg)		Mf/Mo		Rate (1/min)
7/31/95	f 37	600	800	3% O2/N2	1	2.545	2.311		0.908		0.0400
7/31/95	f 38	600	1000	3% O2/N2	1	2.380	2.161		0.908		0.0483
8/1/95	f 39	800	1000	3% O2/N2	15	2.898	2.631		0.908		0.0350
8/1/95	f 40	800	800	3% O2/N2	15	3.920	3.559		0.908		0.0350
8/15/95	f 42	700	800	3% O2/N2	15	2.540	2.304		0.907		0.0300
8/16/95	f 43	650	800	3% O2/N2	15	3.060	2.739		0.895		0.0125
8/17/95	f 44	625	800	3% O2/N2	15	3.360	3.064		0.912		0.0125
8/17/95	f 45	600	800	3% O2/N2	15	3.048	2.926		0.960		0.0214
8/22/95	f 47	600	800	1% O2/N2	1	2.910	2.619		0.900		0.0100
8/22/95	f 48	700	800	0.5% O2/N2	1	3.470	3.151		0.908		0.0059
8/22/95	f 49	700	800	1% O2/N2	1	3.060	2.754		0.900		0.0114
8/23/95	f 50	700	800	3% O2/N2	1	3.920	3.559		0.908		0.0358
8/24/95	f 51	700	800	0.5% O2/N2	1	2.934	2.655		0.905		0.0060
8/24/95	f 52	600	800	0.5% O2/N2	1	2.900	2.633		0.908		0.0056
8/25/95	f 53	800	800	1% O2/N2	1	2.734	2.485		0.909		0.0150
8/28/95	f 54	600	800	1% O2/N2	5	2.572	2.335		0.908		0.0180
8/28/95	f 55	700	800	0.5% O2/N2	5	2.275	2.052		0.902		0.0067
8/29/95	f 56	700	800	1% O2/N2	5	2.284	2.062		0.903		0.0175
8/29/95	f 57	700	800	3% O2/N2	5	2.117	1.916		0.905		0.0400
8/30/95	f 58	700	800	3% O2/N2	5	3.004	2.704		0.900		0.0400
9/1/95	f 59	800	800	1% O2/N2	5	4.310	3.879		0.900		0.0164
9/5/95	f 60	700	800	0.5% O2/N2	15	3.006	2.705		0.900		0.0067
9/6/95	f 61	700	800	1% O2/N2	15	2.436	2.192		0.900		0.0150
9/6/95	f 62	800	800	0.5% O2/N2	1	3.520	3.168		0.900		0.0082
9/7/95	f 63	800	800	3% O2/N2	1	3.034	2.731		0.900		0.0429
9/7/95	f 64	600	800	0.5% O2/N2	5	4.680	4.212		0.900		0.0092
9/8/95	f 65	600	800	3% O2/N2	5	2.916	2.654		0.910		0.0450
9/8/95	f 66	800	800	0.5% O2/N2	5	4.510	4.104		0.910		0.0078
9/11/95	f 67	800	800	3% O2/N2	5	2.791	2.512		0.900		0.0467
9/11/95	f 68	600	800	0.5% O2/N2	15	2.469	2.247		0.910		0.0045
9/12/95	f 69	600	800	1% O2/N2	15	3.195	2.994		0.937		0.0060
9/13/95	f 70	800	800	0.5% O2/N2	15	3.450	3.105		0.900		0.0054
9/22/95	f 75	600	800	1% O2/N2	1	4.600	4.140		0.900		0.0100

was quite small. Complete conversion to $Fe_3(SO_4)_3$ would produce a theoretical value of $M_f/M_o = 2.274$. The final values of $M_f/M_o = 0.960$ from test f45 and $M_f = 0.937$ from test f69 correspond to a final solid product containing only about 4% and 2%, respectively, of $Fe_2(SO_4)_3$.

Reproducibility

Duplicate runs have been competed at three sets of conditions by the end of the quarter, and the reproducibility in each case was almost perfect. These results are summarized in Table 4. Additional reproducibility tests are planned.

Gas Flow Rate

A standard volumetric feed rate of 800 sccm was chosen after a series of scoping tests indicated that, in this flow range, the initial rate was effectively independent of flow rate. All but two of the tests listed in Table 3 used this standard flow rate.

Temperature

The small effect of temperature identified in the atmospheric pressure electrobalance tests has been confirmed. Results showing the initial rate as a function of temperature for three data sets are shown in Figure 17. All data are at 1 atm and results are presented for three different O_2 mol fractions. Apparent activation energies for the three data sets range from about 3300 to 5500 cal/mol, even smaller than the apparent activation energy reported earlier from the atmospheric pressure electrobalance. Results from data sets at higher pressure also show that the effect of temperature is small.

Once again, this result suggests that transport resistances are more important than surface chemistry in determining the global reaction rate.

Pressure

The effect of reaction pressure on the initial reaction rate is shown in Figure 18 for three data sets at the intermediate temperature of 700°C. There appears to be a small increase in initial rate between 1 and 5 atm, followed by a decrease between 5 and 10 atm. The data at 0.5% O_2 in Figure 18 show no significant pressure effect. However results from other data sets not shown are consistent with the initial increase followed by a decrease at high pressure.

This observation is also consistent with the interpretation that the global rate is controlled by transport resistances. If surface controlled, the initial rate at constant temperature and mol fraction should be directly proportional to pressure. In contrast, transport coefficients can, in appropriate situations, decrease with increasing pressure.

Table 4. Reproducibility of the Initial Rate from multiple Tests at the Same Reaction Conditions Using the High Pressure Electrobalance

Temp., °C	Press., atm	Flow Rate, sccm	Mol Fraction	Test No.	Initial Rate, min^{-1}
700	5	800	0.03	f57	0.0400
				f58	0.0400
600	1	800	0.01	f47	0.0100
				f75	0.0100
800	1	800	0.005	f48	0.0059
				f51	0.0060

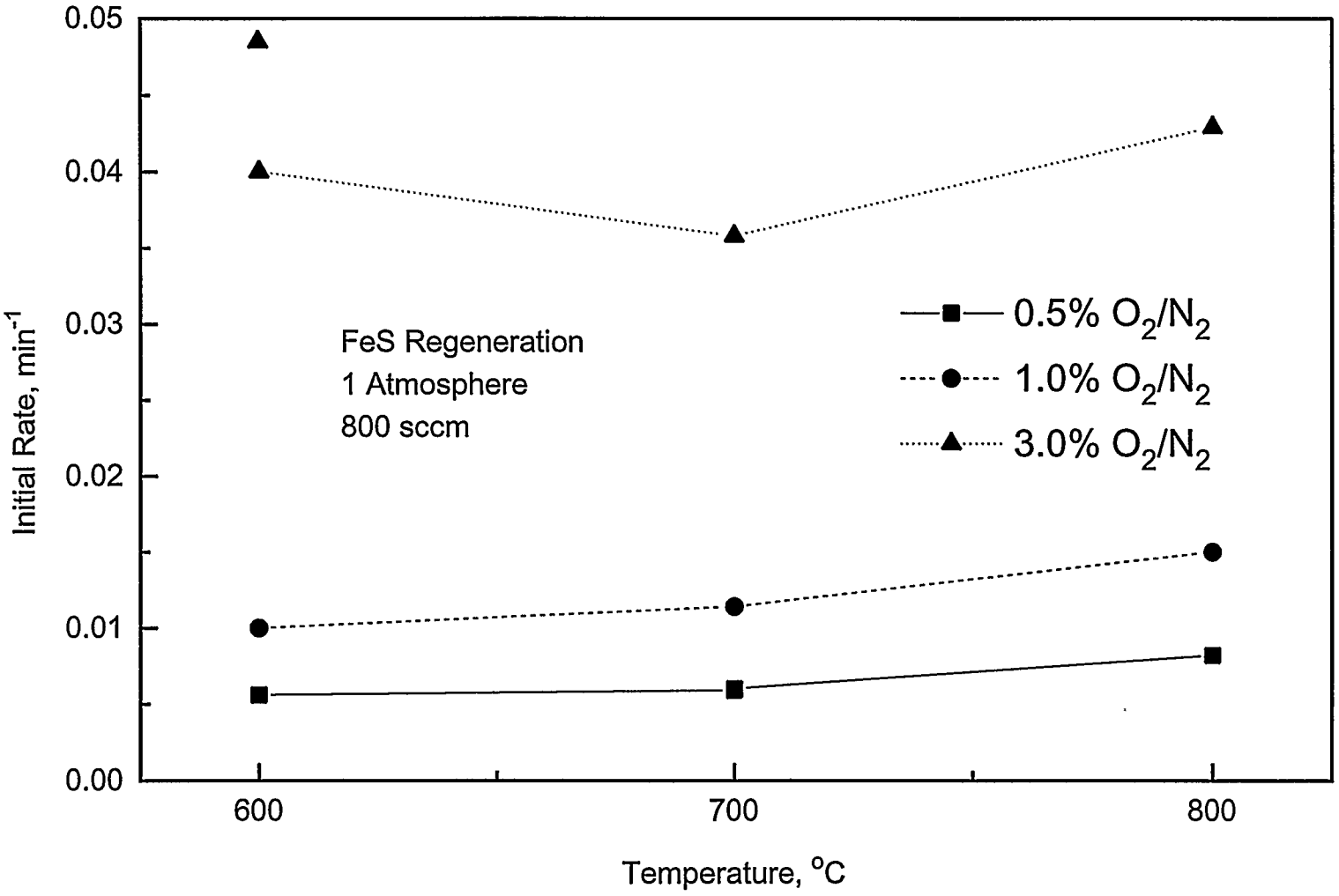

Figure 17. The Effect of Temperature on the initial Reaction Rate for the Regeneration of FeS in O_2/N_2

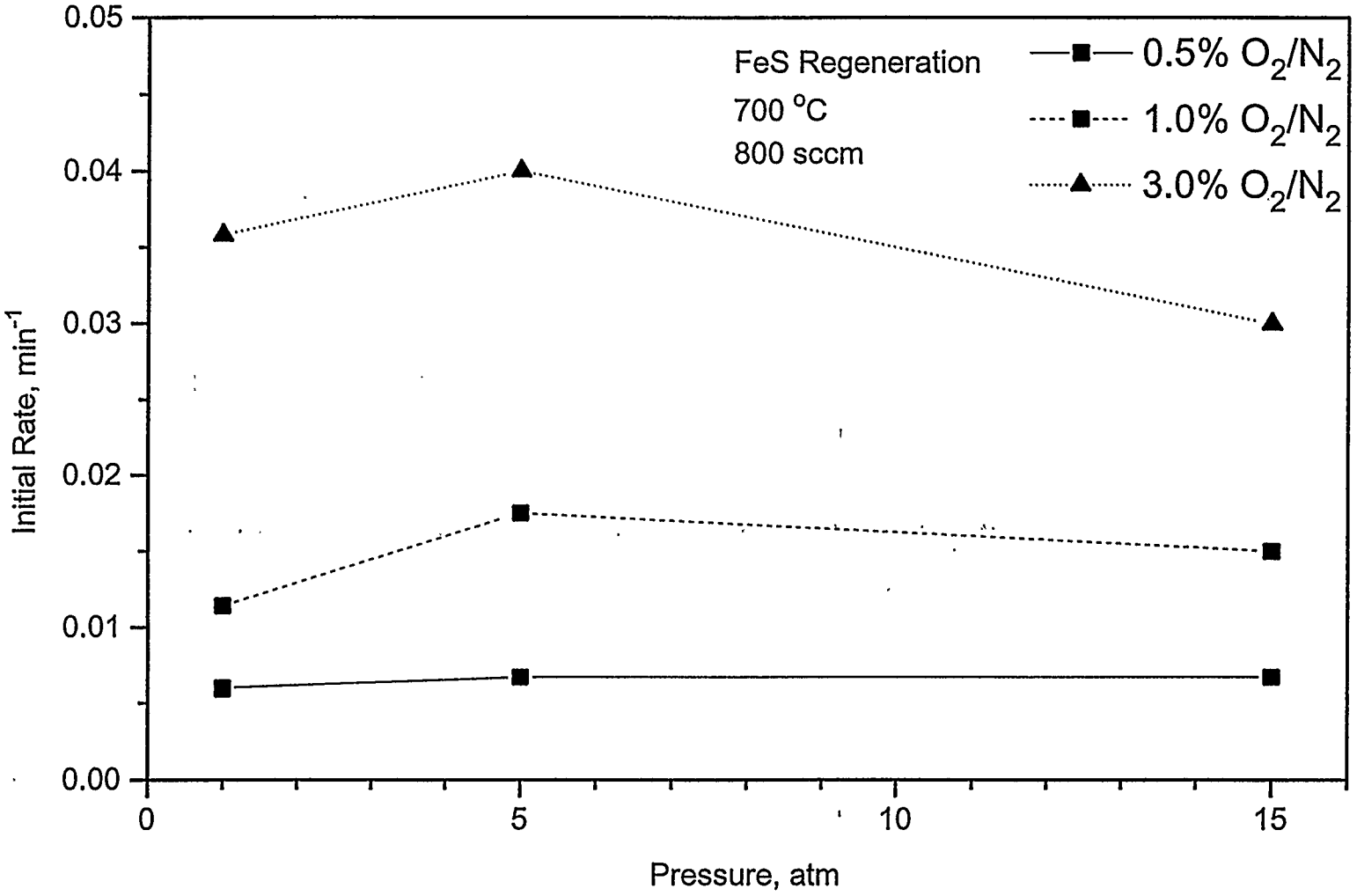

Figure 18. The Effect of Pressure on the Initial Rate for the Regeneration of FeS in O_2/N_2

O_2 Mol Fraction

The initial regeneration rate is directly proportional to the O_2 mol fraction as shown in Figure 19. Three data sets at 5 atm and temperatures of 600, 700, and 800°C are included. The best straight line through the origin is shown for each of the data sets. This data also confirms the small effect of temperature on the global rate.

The pseudo first-order rate constant at each temperature, which is given by the slope of the line is 1.54 at 600°C, 1.35 at 700°C, and 1.56 at 800°C. Correlation coefficients are greater than 0.99 at each temperature. However, visual inspection of the data suggests that the initial rate for the test at 700°C and 3% O_2 may be somewhat low. By ignoring the effect of temperature, it is possible to fit all data in Figure 19 to a single straight line. This straight line has a slope of 1.46 and a correlation coefficient of 0.994.

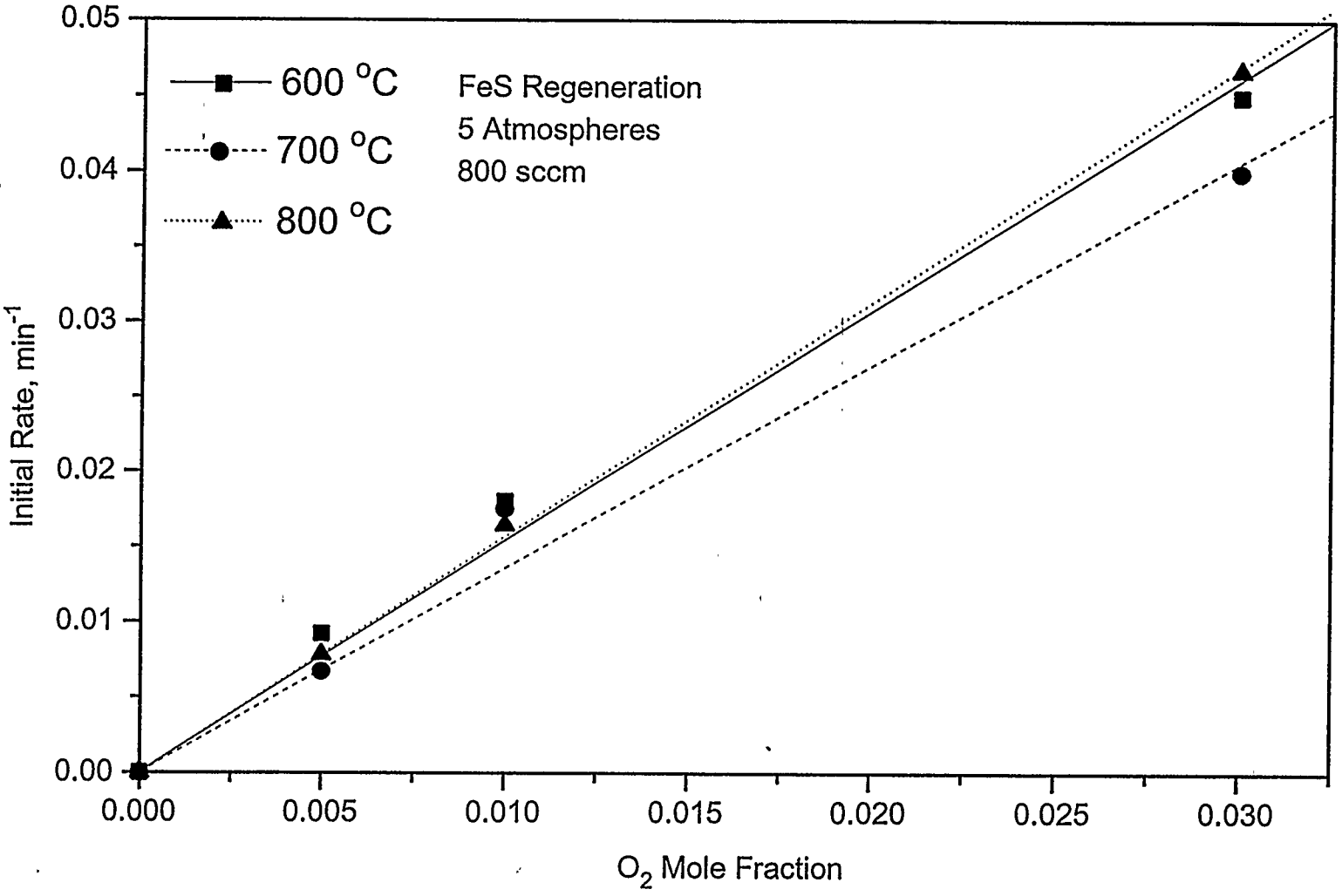

Figure 19. The Effect of O_2 mol Fraction on the Initial Rate for the Regeneration of FeS in O_2/N_2